Electronic excited state transport in solution

C. R. Gochanour,[a] Hans C. Andersen,[b] and M. D. Fayer[c]

Department of Chemistry, Stanford University, Stanford, California 94305
(Received 21 December 1978)

The transport of electronic excitations between randomly distributed sites is examined. The Green function solution to the master equation is expanded as a diagrammatic series. Topological reduction of the series results in an expression for the Green function which is equivalent in form to the Green function solution of a generalized diffusion equation. The diagrammatic technique used suggests an interesting class of self-consistent approximations. This self-consistent method of approximation is applied to the specific case of the Förster transfer rate. The solutions obtained are well-behaved for all times and all site densities and indicate that transport is nondiffusive at short times and diffusive at long times. The mean squared displacement of the excitation and the time derivative of the mean squared displacement are calculated. These calculations illustrate that the time regime in which diffusive transport occurs is dependent on density. For low density systems transport becomes diffusive only at very long time, i.e., more than a few lifetimes. For high densities transport becomes diffusive within one lifetime. The application of the picosecond transient grating technique to the study of this problem is briefly discussed.

I. INTRODUCTION

The transport of electronic excitations has been studied extensively in a wide variety of molecular materials. This phenomenon occurs in pure molecular crystals[1] as well as in mixed crystals,[2] amorphous solids,[3] liquids,[4] and biological systems such as the photosynthetic unit.[5] The bulk of theoretical and detailed experimental work has been directed toward pure crystals since the symmetry properties of the crystal lattice provide considerable aid in reducing the difficulties associated with the many-body problem.[1] In materials other than pure crystals, the molecules of interest are solutes in a solid or liquid solution where the major component, i.e., the host species, does not directly participate in the transfer process. (The host species does provide a dielectric medium and a phonon bath.) In solutions, the molecules have a statistical distribution of intermolecular distances and since the intermolecular interactions responsible for excited state transport are distance dependent,[6] a distribution of transfer rates and pathways exists. This results in a complex problem, in which it is difficult even to determine if transport is diffusive.

Early workers took basically two approaches. For concentrated solutions, it was assumed that molecules are uniformly spaced.[6(a)] The problem reduces to a random walk on a periodic lattice for which transport is diffusive.[7] In the limit of very dilute solutions, a molecule is considered to interact with a single near neighbor.[6(a)] This approach has also been used to describe fluorescence depolarization experiments in dilute solutions; a detailed examination involving clusters of varying sizes has been given by Hemenger and Pearlstein and Knox and Craver.[4]

Recently Haan and Zwanzig[8] attacked the general problem by deriving a formal Green function solution to the master equation and then expanding the Green function in powers of density. The first and second order terms were calculated as an approximation to the complete density expansion. Using this approximation, the time derivative of the average mean squared displacement, $d\langle r^2(t)\rangle/dt$, was calculated. If this quantity is a constant, transport is diffusive. The Haan and Zwanzig results are valid at short times and low concentrations and clearly exhibit nondiffusive behavior at short times. However, due to the nature of the truncated density expansion, the approximation fails at high densities and long times.

The nondiffusive behavior at short times and the possibility of a transition to diffusive behavior at long times can be understood on the basis of the following qualitative arguments. A nonuniform distribution of active molecules can result in a good deal of correlated motion of the excitation among molecules in small clusters formed by statistical variations in number density. By correlated motion, we mean that there is a large probability of an excitation rapidly returning to a previously visited molecule. The correlated motion is short range and nondiffusive. At longer times, the probability distribution in the initial clusters tends toward uniformity, and transfer to more distant molecules becomes important. In this situation transport is expected to be diffusive.

To investigate the nature of energy transport at long times and high concentrations, we have built on the excellent foundation provided by Haan and Zwanzig. Starting with their formal Green function solution, we employ a diagrammatic procedure. A self-consistency equation is derived which permits an excellent approximation to many high order terms in the diagrammatic expansion of the Green function. The result is a solution which is well-behaved at long times and high concentrations as well as at short times and low concentrations. The results of this approximation indicate that at all concentrations, transport becomes diffusive at sufficiently long times. However, at low concentrations, transport does not become diffusive within the first few excited state lifetimes and thus for practical purposes does not become diffusive. At moderate concentrations, transport becomes diffusive within a lifetime. At very high

---

[a] Eastman Kodak Fellow.
[b] Supported provided by NSF Grant No. CHE 78-09317.
[c] Alfred P. Sloan Fellow and Dreyfus Foundation Fellow.

 0021-9606/79/094254-18$01.00

concentrations, transport becomes diffusive at exceedingly short times and rapid diffusion over macroscopic distances occurs. Inherent in the use of the Master Equation is the assumption that energy transport is "incoherent." However in some situations, such as exciton transport in pure molecular crystals at liquid helium temperatures, "coherent" transport can be important.[1(b)] In this case or in any system where there exists well-defined phase relationships between excitations on different sites, alternate approaches such as the "Generalized Master Equation" of Knox and Kenkre[1(c)] or the method of Grover and Silbey[1(d)] are in order. Finally, experimental observables are discussed and it is shown that a picosecond transient grating experiment[2(b)] can be employed to measure the diffusion coefficient in highly concentrated solutions and to investigate the correlated motion in dilute solutions.

II. THE MASTER EQUATION AND GREEN FUNCTION

In order to establish the notation and clearly state the problem we will repeat the initial steps of Haan and Zwanzig's[8] work. The system under consideration consists of N molecules randomly distributed with number density ρ in a volume Ω. Each configuration of the system, denoted by R, is characterized by the locations of the N molecules, $(\mathbf{r}_1, \mathbf{r}_2, \ldots, \mathbf{r}_N)$. The probability that an excitation is found on the jth molecule in configuration R at time t, $p_j'(R, t)$, satisfies the master equation

$$dp_j'(R,t)/dt = -p_j'(R,t)/\tau + \sum_k w_{jk}[p_k'(R,t) - p_j'(R,t)] . \quad (1)$$

τ is the measured lifetime of the excitation and w_{jk} is the transfer rate between molecules j and k. w_{jj} is defined to be zero. To develop the formalism we will leave our results in terms of a general transfer rate $w_{jk}(r_{jk})$ in which, for simplicity, any orientation factors have been neglected. (The orientation factors will be included in a subsequent experimental study.[9]) Ultimately we will apply the formalism to the orientation averaged Förster rate[6]

$$w_{jk} = \tau^{-1}(R_0/r_{jk})^6 . \quad (2)$$

As we will focus our attention on the spatial transport of the excitation, the neglect of orientation factors should not affect the general conclusions of this work.

The substitution

$$p_j(R,t) = p_j'(R,t)\exp(t/\tau) \quad (3)$$

is made to eliminate the decay term and yields the master equation

$$dp_j(R,t)/dt = \sum_k w_{jk}[p_k(R,t) - p_j(R,t)] . \quad (4)$$

If we define the matrix W by

$$W_{jk} = w_{jk} - \delta_{jk}\sum_l w_{kl} , \quad (5)$$

the master equation becomes

$$d\mathbf{p}(R,t)/dt = \mathbf{W}\cdot\mathbf{p}(R,t) , \quad (6)$$

where $\mathbf{p}(R, t)$ is a vector with components $(p_1(R, t), p_2(R, t), \ldots, p_N(R, t))$. The formal solution is given by

$$\mathbf{p}(R,t) = \exp(t\mathbf{W})\cdot\mathbf{p}(R,0) . \quad (7)$$

The initial value $\mathbf{p}(R, 0)$ is determined by the spatial distribution of the excitation pulse, i.e., $p_j(R, 0)$ is only a function of $\mathbf{r}_j$,

$$p_j(R,0) = F(\mathbf{r}_j) . \quad (8)$$

Information concerning transport in the system will be obtained from the ensemble average density of excitations

$$P(\mathbf{r},t) = \left\langle \sum_j \delta(\mathbf{r}_j - \mathbf{r}) p_j(R,t) \right\rangle , \quad (9)$$

where the ensemble average of a function $A(R)$ is defined by

$$\langle A(R)\rangle = \frac{1}{\Omega^N}\int_\Omega d\mathbf{r}_1 \cdots \int_\Omega d\mathbf{r}_N A(R) . \quad (10)$$

$P(\mathbf{r}, t)$ will be written in terms of a Green function

$$P(\mathbf{r},t) = \int d\mathbf{r}' G(\mathbf{r},\mathbf{r}',t)P(\mathbf{r}',0) , \quad (11)$$

where

$$G(\mathbf{r},\mathbf{r}',t) = \rho^{-1}\left\langle \sum_j \sum_k \delta(\mathbf{r}_j - \mathbf{r})\delta(\mathbf{r}_k - \mathbf{r}')[\exp(t\mathbf{W})]_{jk} \right\rangle \quad (12)$$

and

$$P(\mathbf{r}',0) = \left\langle \sum_j \delta(\mathbf{r}_j - \mathbf{r}')F(\mathbf{r}_j) \right\rangle = \rho F(\mathbf{r}') . \quad (13)$$

The sum over j and k in Eq. (12) contains only two distinct types of terms, $j = k$ and $j \neq k$. Thus the Green function can be written as

$$G(\mathbf{r},\mathbf{r}',t) = G^s(\mathbf{r},\mathbf{r}',t) + G^m(\mathbf{r},\mathbf{r}',t). \quad (14)$$

$G^s(\mathbf{r}, \mathbf{r}', t)$ is the sum of the N terms in Eq. (12) with $j = k$ ($j = 1$ chosen arbitrarily) and is given by

$$G^s(\mathbf{r},\mathbf{r}',t) = (N/\rho)\langle\delta(\mathbf{r}_1 - \mathbf{r})\delta(\mathbf{r}_1 - \mathbf{r}')[\exp(t\mathbf{W})]_{11}\rangle = \delta(\mathbf{r} - \mathbf{r}')\langle[\exp(t\mathbf{W})]_{11}\rangle . \quad (15)$$

$G^s(\mathbf{r}, \mathbf{r}', t)$ is only a function of relative position $\mathbf{r} - \mathbf{r}'$. The integral of $G^s(\mathbf{r}, \mathbf{r}', t)$ over a small volume about $\mathbf{r}'$ is the probability of finding the excitation on the site of initial excitation at time t. The choice of $j = 1$ in the derivation of Eq. (15) labels the initial site as molecule 1. The $N(N-1)$ terms with $j \neq k$ are summed to yield the function $G^m(\mathbf{r}, \mathbf{r}', t)$ which is defined by ($k = 1$, $j = 2$ chosen arbitrarily)

$$G^m(\mathbf{r},\mathbf{r}',t) = (N-1)(N/\rho)\langle\delta(\mathbf{r}_2 - \mathbf{r})\delta(\mathbf{r}_1 - \mathbf{r}')[\exp(t\mathbf{W})]_{12}\rangle = (N-1)\langle\delta(\mathbf{r}_{12} - \mathbf{r} + \mathbf{r}')[\exp(t\mathbf{W})]_{12}\rangle . \quad (16)$$

Like $G^s(\mathbf{r} - \mathbf{r}', t)$, $G^m(\mathbf{r}, \mathbf{r}', t)$ is a function of relative position. The integral of $G^m(\mathbf{r} - \mathbf{r}', t)$ over a small volume about $\mathbf{r}$ is the probability of finding the excitation at $\mathbf{r}$ at time t given that the excitation is initially at $\mathbf{r}'$. The choice of $k = 1$ and $j = 2$ labels the site of initial excitation as molecule 1 and the molecule at $\mathbf{r}$ as molecule 2.

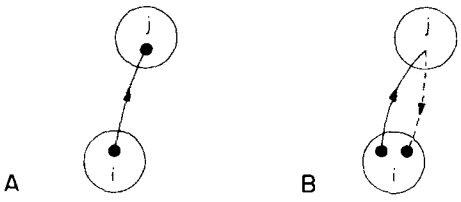

FIG. 1. The diagrammatic structure associated with a factor of w_{ij} (A) and $-w_{ij}$ (B).

At this point in the calculation Haan and Zwanzig[8] express $G(\mathbf{r}-\mathbf{r}', t)$ and its thermodynamic limit as density expansions. The lowest order terms in the expansion are obtained for the Förster rate to yield a result which is accurate for low density. A scaling argument is used to show that this result is also valid at short time. The scaling law also shows that an approximation to the Green function which is valid for high density is also valid at long time. The short time–low density solution indicates that transport is nondiffusive, with the mean squared displacement going as $t^{5/6}$. For high density, the density expansion is no longer appropriate and therefore the nature of transport for high density and long time could not be determined.

III. DIAGRAMMATIC EXPANSION OF THE GREEN FUNCTION

To obtain a more complete description, containing both the long time high density and short time low density behavior, we will derive diagrammatic expansions for $G^s(\mathbf{r}-\mathbf{r}', t)$ and $G^m(\mathbf{r}-\mathbf{r}', t)$ in the thermodynamic limit. A similar approach was used by Haan[10] to study this problem, however a result accurate in the high density–long time regime was not obtained. It will be convenient to work with Laplace–Fourier transforms. The transform of $F(\mathbf{r}, t)$, $\hat{F}(\mathbf{k}, \epsilon)$, is defined by

$$\hat{F}(\mathbf{k}, \epsilon) = \int_0^\infty dt \exp(-\epsilon t) \int d\mathbf{r} \exp(i\mathbf{k}\cdot\mathbf{r}) F(\mathbf{r}, t) . \tag{17}$$

As was shown earlier $G(\mathbf{r}-\mathbf{r}', t)$ can be written as the sum of $G^s(\mathbf{r}-\mathbf{r}', t)$ and $G^m(\mathbf{r}-\mathbf{r}', t)$. Thus the transform of the Green function, $\hat{G}(\mathbf{k}, \epsilon)$, can be written as

$$\hat{G}(\mathbf{k}, \epsilon) = \hat{G}^s(\mathbf{k}, \epsilon) + \hat{G}^m(\mathbf{k}, \epsilon) . \tag{18}$$

$\hat{G}^s(\mathbf{k}, \epsilon)$ is in fact independent of $\mathbf{k}$. From Eq. (15) we have

$$\hat{G}^s(\epsilon) = \langle [(\epsilon - \mathbf{W})^{-1}]_{11} \rangle . \tag{19}$$

Transforming Eq. (16) yields

$$\hat{G}^m(\mathbf{k}, \epsilon) = (N-1)\langle \exp(i\mathbf{k}\cdot\mathbf{r}_{12}) [(\epsilon - \mathbf{W})^{-1}]_{12} \rangle . \tag{20}$$

We begin by considering $\hat{G}^s(\epsilon)$. If the identity

$$(\epsilon - \mathbf{W})^{-1} = \epsilon^{-1} + \epsilon^{-1}\cdot\mathbf{W}\cdot(\epsilon - \mathbf{W})^{-1} \tag{21}$$

is iterated we obtain the expansion

$$(\epsilon - \mathbf{W})^{-1} = \epsilon^{-1} + \epsilon^{-1}\cdot\mathbf{W}\cdot\epsilon^{-1} + \epsilon^{-1}\cdot\mathbf{W}\cdot\epsilon^{-1}\cdot\mathbf{W}\cdot\epsilon^{-1} + \cdots . \tag{22}$$

This expansion is substituted into Eq. (19) to obtain the following expansion of $\hat{G}^s(\epsilon)$ in powers of W

$$\begin{aligned}\hat{G}^s(\epsilon) &= \epsilon^{-1} + \langle (\epsilon^{-1}\cdot\mathbf{W}\cdot\epsilon^{-1})_{11} \rangle \\ &\quad + \langle (\epsilon^{-1}\cdot\mathbf{W}\cdot\epsilon^{-1}\cdot\mathbf{W}\cdot\epsilon^{-1})_{11} \rangle + \cdots \\ &= \epsilon^{-1} + \sum_{n=1}^{\infty} (1/\epsilon^{n+1}) \langle (\mathbf{W}^n)_{11} \rangle .\end{aligned} \tag{23}$$

If we write out the matrix product explicitly the nth order term in this expansion is given by

$$(1/\epsilon^{n+1})\langle (\mathbf{W}^n)_{11} \rangle = \sum_{i,j,\ldots,k} (1/\epsilon^{n+1}) \langle W_{1i} W_{ij} \cdots W_{k1} \rangle . \tag{24}$$

Each product in this series is characterized by an ordered set of $n-1$ subscripts, $(i, j, \ldots, k)$. If the definition of W_{ij} from Eq. (5) is substituted into a given product, a series of products of w_{ij} factors results

$$\begin{aligned}(1/\epsilon^{n+1})\langle W_{1i} W_{ij} \cdots W_{k1} \rangle &= (1/\epsilon^{n+1}) \Big\langle \Big[w_{1i} + \delta_{1i} \sum_{q\neq i} (-w_{iq}) \Big] \\ &\times \Big[w_{ij} + \delta_{ij} \sum_{r\neq j} (-w_{jr}) \Big] \cdots \Big[w_{k1} + \delta_{k1} \sum_{s\neq 1} (-w_{1s}) \Big] \Big\rangle .\end{aligned} \tag{25}$$

A product of n W_{ij}'s, m of which are diagonal elements, generates a series of $(N-1)^m$ products of n w_{ij} factors. Each of these products of w_{ij} factors can be represented by a diagram constructed in the following way: Molecule i will be represented by a circle labeled i. Each factor of w_{ij} is represented by a solid arrow from circle i to circle j, as in Fig. 1(A), which can be interpreted as the increase in probability on j due to transfer from i. A factor of $-w_{ij}$ is represented by a solid arrow from i to j followed by a dashed arrow back to i, as in Fig. 1(B), and corresponds to the decrease in probability on i due to transfer to j. The diagram representing a product of w_{ij} factors is constructed by joining the arrows for consecutive w_{ij} or $-w_{ij}$ factors head to tail. A point at which two arrows are joined will be called a vertex if the arrow coming out of the point is a solid arrow. The beginning and end points of the diagram will also be called vertices. A vertex will be indicated by a solid dot in the diagram. For example, the third order term in Eq. (23) contains the product $W_{12}W_{22}W_{21}$ which corresponds to $N-1$ w_{ij} products including $w_{12}(-w_{23})w_{21}$ and $w_{12}(-w_{21})w_{21}$. The corresponding diagrams are shown in Fig. 2. Note that a point with a solid arrow coming in and a dashed arrow coming out is not a vertex and is not drawn as a solid dot. To keep track of the $(n+1)$ ϵ^{-1} factors associated with a product of n w_{ij} factors, a factor of ϵ^{-1} is associated with each vertex. The reason for this procedure will be made apparent in the discussion of the topological reduction of the diagrammatic series in Sec. III. Each product begins with a w_{1i} or $-w_{1i}$ factor and ends with a w_{k1} or $-w_{k1}$ factor and therefore each diagram begins with a solid arrow

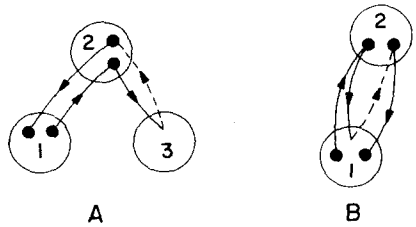

FIG. 2. The diagrams representing the products $w_{12}(-w_{23})w_{21}$ (A) and $w_{12}(-w_{21})w_{21}$ (B).

leaving circle 1 and ends with a solid or dashed arrow into circle 1. The allowed first factors in a w_{ij} product are generated by the sum over i in Eq. (25). The $N-1$ terms with $i \neq 1$ correspond to a beginning factor of w_{1i}, where $i = 2, 3, \ldots, N$, while the $i = 1$ term corresponds to beginning factors $-w_{1i}$, with $i = 2, 3, \ldots, N$. Thus the diagram can begin with either a solid arrow from circle 1 to any other circle or a solid arrow from circle 1 to any other circle followed by a dashed arrow back to circle 1. The sum over j in Eq. (25) allows us to continue each of these diagrams by connecting the ith circle, which may be circle 1, with any other circle with either a solid arrow or a solid arrow followed by a dashed arrow back to i. This process continues through the n sums in Eq. (25) and leads to the conclusion that the nth order term in Eq. (23) can be represented by all diagrams with a continuous path of solid and dashed arrows beginning on the root circle, circle 1, passing through intermediate circles, and ending on the root circle. Each diagram must contain a total of n solid arrows and a dashed arrow may only return to the circle from which the previous solid arrow began; two dashed arrows may not be placed in succession. The set of intermediate circles will contain circles other than the root circle, which are called the field circles, and possibly the root circle itself. A vertex is associated with the beginning and end of each arrow that is not the beginning of a dashed arrow.

The value of a diagram is obtained by performing an ensemble average of the product formed by a factor of ϵ^{-1} for each vertex, a factor of w_{ij} for each solid arrow, and a factor of -1 for each dashed arrow. Thus the value of a diagram is

$$\frac{1}{\Omega^N \epsilon^{n+1}} \int_\Omega d\mathbf{r}_1 \cdots \int_\Omega d\mathbf{r}_N \prod w_{ij} \prod (-1), \tag{26}$$

where Πw_{ij} and $\Pi(-1)$ represent the appropriate products of w_{ij} and -1 factors. As w_{ij} is a function of the relative position, the integrand depends only on the position of the molecules represented by the m field circles relative to molecule 1, i.e., the value of a diagram can be written as

$$\frac{1}{\Omega^m \epsilon^{n+1}} \int_\Omega d\mathbf{r}_{1i} \cdots \int_\Omega d\mathbf{r}_{1k} \prod w_{ij} \prod (-1). \tag{27}$$

The value of a diagram does not depend on the labels assigned to the field circles. For a diagram with m field circles there are $(N-1)(N-2)\cdots(N-m)$ numerically equal diagrams. To simplify the diagrammatic series we can construct the diagrams without labels on the field circles, keep only distinct diagrams, assign labels arbitrarily, and multiply the value given by (27) by $(N-1)(N-2)\cdots(N-m)$. Two unlabeled diagrams are distinct if, when labeled with the same set of labels, there is no way of rearranging labels to make the diagrams identical.

$\hat{G}^s(\epsilon)$ can now be written as the diagrammatic series defined by

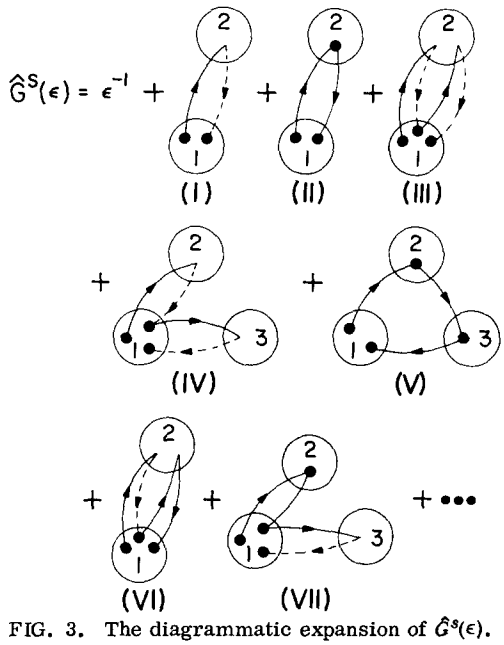

FIG. 3. The diagrammatic expansion of $\hat{G}^s(\epsilon)$. Each diagram contains a continuous path of solid and dashed arrows beginning and ending on circle 1. The diagrams shown represent all w_{ij} products in Eq. (23) for $n \leq 2$ (diagrams I–IV) and examples of diagrams for $n = 3$ (diagrams V–VII). The value of a diagram is given by (29).

$$\hat{G}^s(\epsilon) = \langle [(\epsilon - \mathbf{W})^{-1}]_{11} \rangle$$

$$= \epsilon^{-1} + \text{The sum of all distinct diagrams which have a path of solid and dashed arrows beginning and ending on circle 1.} \tag{28}$$

The restrictions concerning the allowed sequences of solid and dashed arrows and the location of vertices noted earlier all apply. A diagram with m field circles will be labeled with the set of labels $(2, 3, \ldots, m+1)$. The value of an nth order diagram with m field circles is

$$\frac{(N-1)!}{(N-m-1)!\,\Omega^m \epsilon^{n+1}} \int_\Omega d\mathbf{r}_{12} \cdots \int_\Omega d\mathbf{r}_{1m+1} \prod w_{ij} \prod (-1), \tag{29}$$

where a factor of w_{ij} appears in Πw_{ij} for each solid arrow connecting circles i and j and a factor of -1 appears in $\Pi(-1)$ for each dashed arrow. Note that in the thermodynamic limit ($N, \Omega \to \infty$, ρ constant)

$$(N-1)!/[(N-m-1)!\,\Omega^m] = \rho^m . \tag{30}$$

The diagrams in $\hat{G}^s(\epsilon)$ are shown in Fig. 3. To demonstrate the equivalence of the algebraic series given by Eq. (23) and the diagrammatic series of Eq. (28), we will calculate the first and second order terms in Eq. (23). The first order term is

$$\epsilon^{-2}\langle W_{11} \rangle = \epsilon^{-2} \left\langle \sum_{i \neq 1} (-w_{1i}) \right\rangle . \tag{31}$$

As all particles are identical, this term can be written as

$$\epsilon^{-2}\langle W_{11} \rangle = \epsilon^{-2}(N-1)\langle -w_{12} \rangle$$

$$= \frac{N-1}{\Omega \epsilon^2} \int_\Omega d\mathbf{r}_{12}(-w_{12}) . \tag{32}$$

Applying the rules for evaluation of a $\hat{G}^s(\epsilon)$ diagram to

the first order diagram, diagram (I) in Fig. 3, yields the same result. The second order term in Eq. (23) is

$$\epsilon^{-3}\langle (W^2)_{11}\rangle = \sum_i \epsilon^{-3}\langle W_{1i} W_{i1}\rangle \ . \tag{33}$$

The terms in the sum with $i \neq 1$ are given by

$$\sum_{i\neq 1} \epsilon^{-3}\langle W_{1i} W_{i1}\rangle = \sum_{i\neq 1} \epsilon^{-3}\langle w_{1i} w_{i1}\rangle \ . \tag{34}$$

All terms in this sum are equal, so

$$\sum_{i\neq 1} \epsilon^{-3}\langle w_{1i} w_{i1}\rangle = \epsilon^{-3}(N-1)\langle w_{12} w_{21}\rangle = \frac{N-1}{\epsilon^3 \Omega} \int_\Omega d\mathbf{r}_{12} w_{12} w_{21} \ . \tag{35}$$

This is the value of diagram (II) in Fig. 3. For $i=1$ in Eq. (33) the W product can be divided into two types of w_{ij} product since

$$\epsilon^{-3}\langle W_{11}^2\rangle = \sum_{j\neq 1}\sum_{k\neq 1} \epsilon^{-2}\langle (-w_{1j})(-w_{1k})\rangle \ . \tag{36}$$

For $j=k$ we have

$$\sum_{j\neq 1} \epsilon^{-3}\langle (-w_{1j})(-w_{1j})\rangle = \frac{N-1}{\epsilon^3\Omega} \int_\Omega d\mathbf{r}_{12}(-w_{12})(-w_{12}), \tag{37}$$

which is the value of diagram (III) in Fig. 3. The terms with $j \neq k$ in Eq. (36) are all equal and, when summed, yield the value of the final second order diagram, diagram (IV) in Fig. 3,

$$\sum_{j\neq 1}\sum_{k\neq 1,\, k\neq j} \langle (-w_{1j})(-w_{1k})\rangle = \frac{(N-1)(N-2)}{\epsilon^2\Omega^2} \int_\Omega d\mathbf{r}_{12} \int_\Omega d\mathbf{r}_{13}(-w_{12})(-w_{13}) . \tag{38}$$

A similar diagrammatic series can be derived for $\hat{G}^m(\mathbf{k}, \epsilon)$. If we substitute the expansion of $(\epsilon - W)^{-1}$ given by Eq. (22) into Eq. (20) we get

$$\hat{G}^m(\mathbf{k},\epsilon) = \sum_{n=1}^{\infty} \frac{N-1}{\epsilon^{n+1}} \langle \exp(i\mathbf{k}\cdot \mathbf{r}_{12})(\mathbf{W}^n)_{12}\rangle = \sum_{n=1}^{\infty} \sum_{i,j,\cdots,k} \frac{N-1}{\epsilon^{n+1}} \langle \exp(i\mathbf{k}\cdot \mathbf{r}_{12}) W_{1i} W_{ij} \cdots W_{k2}\rangle . \tag{39}$$

Each term in the multiple sum can be written as $(N-1)^m$ products of w_{ij} factors, where m is the number of W_{ii} factors in the product $W_{1i} W_{ij} \cdots W_{k2}$. For the general term we have

$$\langle \exp(i\mathbf{k}\cdot \mathbf{r}_{12}) W_{1i} W_{ij} \cdots W_{k2}\rangle = \left\langle \exp(i\mathbf{k}\cdot \mathbf{r}_{12}) \left[w_{1i} + \delta_{1i} \sum_{q\neq i} (-w_{iq}) \right] \times \left[w_{ij} + \delta_{ij} \sum_{r\neq j} (-w_{jr}) \right] \cdots \left[w_{k2} + \delta_{k2} \sum_{s\neq 2} (-w_{2s}) \right] \right\rangle . \tag{40}$$

To express each of the w_{ij} products as a diagram we follow the procedure developed in the diagrammatic expansion of $\hat{G}^s(\epsilon)$. Each w_{ij} factor is represented by a solid arrow connecting circles i and j and each $-w_{ij}$ factor is represented by a solid arrow from circle i to j followed by a dashed arrow back to i. The form of each product given in Eq. (40) and the definition of the diagrammatic structures for w_{ij} and $-w_{ij}$ results in each arrow into circle i being followed by an arrow leaving circle i. The diagram for a w_{ij} product is constructed by joining arrows in a head to tail fashion. Each product begins with a w_{1i} or $-w_{1i}$ factor and ends with a w_{i2} or $-w_{2i}$ factor and therefore each diagram begins with a solid arrow leaving circle 1 and ends with a solid or dashed arrow into circle 2. Circles 1 and 2 will be designated as root circles and the remaining circles as field circles.

As was shown in detail for the $\hat{G}^s(\epsilon)$ series the sums over $i, j, \ldots, k$ in Eq. (39) result in the association of the nth order term in Eq. (39) with all diagrams which have a path of solid and dashed arrows beginning on circle 1 and ending on circle 2. The path must satisfy all restrictions on the allowed sequence of arrows and contain a total of n solid arrows. The diagrams represent allowed paths of excitation transfer which result in transfer of excitation probability from molecule 1 to molecule 2. The Fourier transform is obtained by including a factor of $\exp(i\mathbf{k}\cdot \mathbf{r}_{12})$ in the value of the diagram.

The value of a diagram in the $\hat{G}^m(\mathbf{k}, \epsilon)$ series is given by $N-1$ multiplied by the ensemble average of: $\exp(i\mathbf{k}\cdot \mathbf{r}_{12})$ multiplied by a factor of w_{ij} for each solid arrow, a factor of -1 for each dashed arrow, and a factor of ϵ^{-1} for each vertex. The transfer rate depends on relative position so we can write the value of an nth order diagram with m field circles as

$$\frac{N-1}{\epsilon^{n+1}} \left\langle \exp(i\mathbf{k}\cdot \mathbf{r}_{12}) \prod w_{ij} \prod (-1) \right\rangle = \frac{N-1}{\epsilon^{n+1}\Omega^{m+1}} \int_\Omega d\mathbf{r}_{12} \int_\Omega d\mathbf{r}_{1i} \cdots \int_\Omega d\mathbf{r}_{1k} \times \exp(i\mathbf{k}\cdot \mathbf{r}_{12}) \prod w_{ij} \prod (-1) . \tag{41}$$

As the value of a diagram does not depend on the labels on the field circles we can simplify the $\hat{G}^m(\mathbf{k}, \epsilon)$ by keeping only distinct diagrams and multiplying the diagram value by a counting factor to account for equivalent diagrams. For a diagram with m field circles there are $(N-2)(N-3)\cdots(N-m-1)$ equivalent diagrams. We can now define $\hat{G}^m(\mathbf{k}, \epsilon)$ by the diagrammatic series:

$\hat{G}^m(\mathbf{k}, \epsilon)$ = The sum of all distinct diagrams with two root circles labeled 1 and 2 and zero or more field circles that have a path of solid and dashed arrows starting on circle 1 and ending on circle 2. (In calculating the value of a diagram, each vertex is assigned a factor of ϵ^{-1}.) (42)

The m field circles will be labeled with the set of labels $(3, 4, \ldots, m+2)$. The value of a diagram in the series is given by

$$\frac{(N-1)!}{(N-m-2)!\,\epsilon^{n+1}\Omega^{m+1}} \int_\Omega d\mathbf{r}_{12} \cdots \int_\Omega d\mathbf{r}_{1m+2} \times \exp(i\mathbf{k}\cdot \mathbf{r}_{12}) \prod w_{ij} \prod (-1) . \tag{43}$$

In the thermodynamic limit

$$(N-1)!/[(N-m-2)!\,\Omega^{m+1}] = \rho^{m+1} . \tag{44}$$

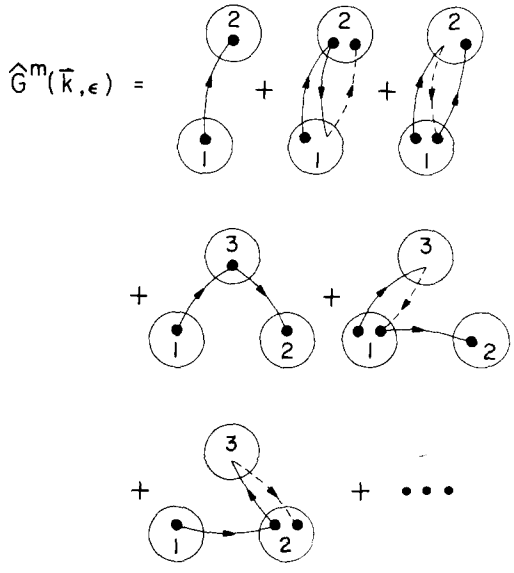

FIG. 4. The diagrammatic expansion of $\hat{G}^m(\mathbf{k},\epsilon)$ [Eq. (42)]. Each diagram contains a continuous path of solid and dashed arrows beginning on circle 1 and ending on circle 2. The value of a diagram is given by (43).

The first and second order diagrams in the series for $\hat{G}^m(\mathbf{k},\epsilon)$ are shown in Fig. 4.

IV. TOPOLOGICAL REDUCTION OF THE $\hat{G}^m(\mathbf{k},\epsilon)$ SERIES IN THE THERMODYNAMIC LIMIT

To simplify the $\hat{G}^m(\mathbf{k},\epsilon)$ series we first note that some of the diagrams in the series contain loops. A loop is a part of a diagram having the following properties. The loop is a sequence of arrows that begins and ends on vertices in the same circle. The circles visited by the path of arrows in the loop are visited in no other part of the diagram. The loop does not pass through a root circle unless it begins and ends on that root circle. Examples of $\hat{G}^m(\mathbf{k},\epsilon)$ diagrams containing loops are shown in Fig. 5(A). Diagrams I and II contain a single loop, beginning at the vertex labeled α and ending at the vertex labeled β. Diagram III is an example of a diagram containing two consecutive loops, one which begins at α and ends at β and one which begins at β and ends at γ. From the definition of a loop we see that if the end vertex of one loop is the beginning of a second loop then the combination of the two loops is itself a loop. If we define a maximal loop as a loop which is not part of a larger loop, each diagram has a unique set of maximal loops that have no arrows or vertices in common.

If a diagram in the $\hat{G}^m(\mathbf{k},\epsilon)$ series has a loop we can imagine constructing a new diagram by erasing each maximal loop and merging the beginning and end vertices of the loop into a single vertex. The resulting diagram will be a different diagram from the $\hat{G}^m(\mathbf{k},\epsilon)$ series. If this process is applied to any of the three diagrams in Fig. 5(A), the diagram shown in Fig. 5(B) results.

We can express the value of a diagram with loops in terms of the value of the diagram with loops removed. The value of the diagram given in Fig. 5(B) is

$$\mathrm{IV}(\mathbf{k},\epsilon)=\rho^2\int d\mathbf{r}_{12}\exp(i\mathbf{k}\cdot\mathbf{r}_{12})\int d\mathbf{r}_{13}\epsilon^{-1}w_{13}\epsilon^{-1}w_{32}\epsilon^{-1}\,. \quad (45)$$

This diagram is the result of removing the loop from diagram I in Fig. 5(A) for which the value is

$$\begin{aligned}\mathrm{I}(\mathbf{k},\epsilon)&=\rho^3\int d\mathbf{r}_{12}\exp(i\mathbf{k}\cdot\mathbf{r}_{12})\\&\quad\times\int d\mathbf{r}_{13}\int d\mathbf{r}_{14}\epsilon^{-1}w_{13}\epsilon^{-1}(-w_{34})\epsilon^{-1}w_{32}\epsilon^{-1}\\&=\rho^2\int d\mathbf{r}_{12}\exp(i\mathbf{k}\cdot\mathbf{r}_{12})\\&\quad\times\int d\mathbf{r}_{13}\epsilon^{-1}w_{13}\left[\rho\int d\mathbf{r}_{34}\epsilon^{-1}(-w_{34})\epsilon^{-1}\right]w_{32}\epsilon^{-1}\,.\end{aligned} \quad (46)$$

If we compare the value of diagram I to that of diagram IV we see that the value of diagram I can be generated by replacement of the ϵ^{-1} factor associated with the vertex in circle 3 in the value of diagram IV by the quantity in brackets in Eq. (46). Similarly the value of diagram II,

$$\begin{aligned}\mathrm{II}(\mathbf{k},\epsilon)&=\rho^4\int d\mathbf{r}_{12}\exp(i\mathbf{k}\cdot\mathbf{r}_{12})\int d\mathbf{r}_{13}\int d\mathbf{r}_{14}\int d\mathbf{r}_{15}\\&\quad\times\epsilon^{-1}w_{14}\epsilon^{-1}w_{45}\epsilon^{-1}(-w_{54})\epsilon^{-1}w_{51}\epsilon^{-1}w_{13}\epsilon^{-1}w_{32}\epsilon^{-1}\\&=\rho^2\int d\mathbf{r}_{12}\exp(i\mathbf{k}\cdot\mathbf{r}_{12})\int d\mathbf{r}_{13}\left[\rho^2\int d\mathbf{r}_{14}\int d\mathbf{r}_{15}\right.\\&\quad\left.\times\epsilon^{-1}w_{14}\epsilon^{-1}w_{45}\epsilon^{-1}(-w_{54})\epsilon^{-1}w_{51}\epsilon^{-1}\right]w_{13}\epsilon^{-1}w_{32}\epsilon^{-1}\end{aligned} \quad (47)$$

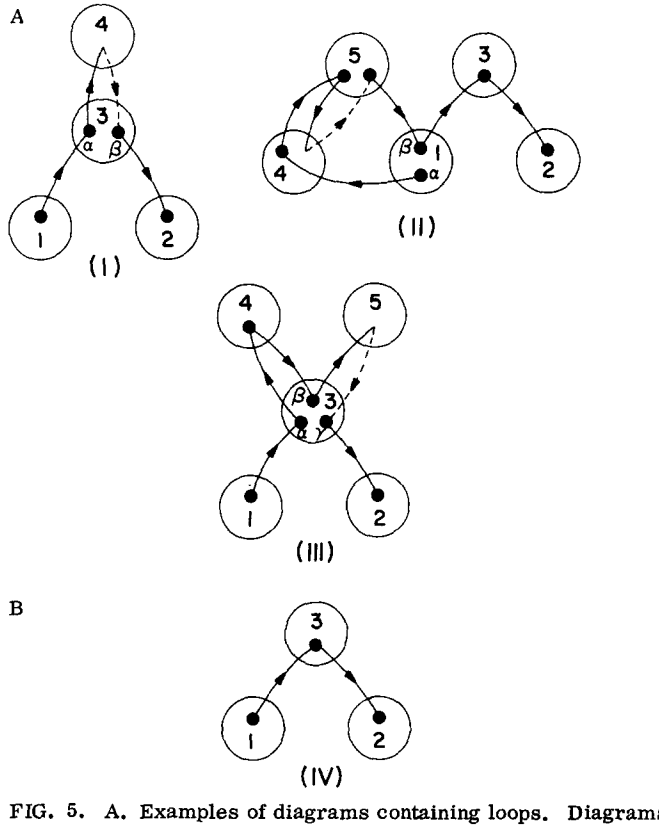

FIG. 5. A. Examples of diagrams containing loops. Diagrams I and II contain a single loop, beginning at vertex α and ending at vertex β. Diagram III contains two consecutive loops, one which begins at α and ends at β and one which begins at β and ends at γ. The path of arrows beginning at α and ending at γ is also a loop, the maximal loop for the diagram. If the maximal loop is removed from each of the diagrams in (A), the diagram shown in 5(B) results.

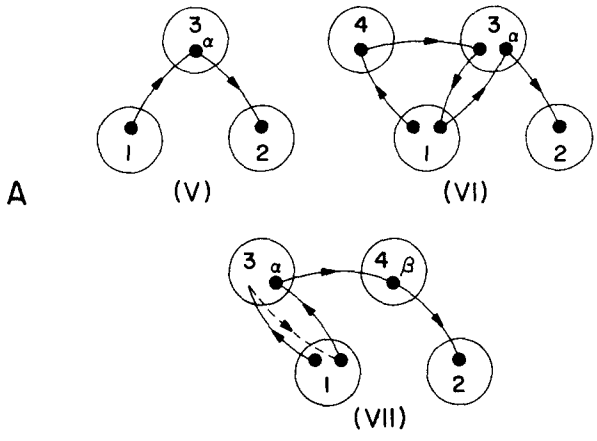

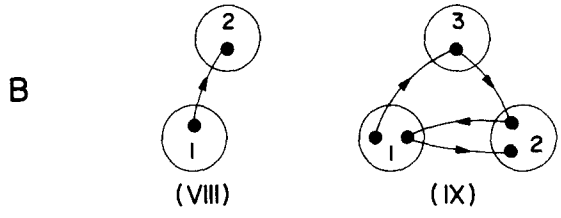

FIG. 6. (A) Examples of diagrams containing nodes. The nodes are labeled with Greek letters. (B) The diagrams from which diagrams V and VI can be constructed. Diagram V is constructed by joining diagram VIII to itself head to tail. Diagram VI is constructed by joining diagrams IX and VIII head to tail.

can be obtained by the replacement of the ϵ^{-1} factor associated with the first vertex of diagram IV by the quantity in brackets in Eq. (47). ϵ^{-1} and the quantities in brackets in Eqs. (46) and (47) are in fact contributions to the $\hat{G}^s(\epsilon)$ series, the quantity in brackets in (46) is the value of diagram I in Fig. 3 and the quantity in brackets in (47) is the value of a fourth order diagram in $\hat{G}^s(\epsilon)$. Examination of the topological structure of a loop and a diagram in the $\hat{G}^s(\epsilon)$ series also results in the conclusion that these structures are identical. If we only consider diagrams in the $\hat{G}^m(\mathbf{k}, \epsilon)$ series that have no loops and replace each ϵ^{-1} factor by $\hat{G}^s(\epsilon)$ we will generate all diagrams in $\hat{G}^m(\mathbf{k}, \epsilon)$. Thus we can conclude that

$\hat{G}^m(\mathbf{k}, \epsilon)$ = The sum of all distinct diagrams with two root circles labeled 1 and 2, zero or more field circles, no loops, and that have a path of solid and dashed arrows starting on circle 1 and ending on circle 2. [In calculating the value of a diagram, each vertex is assigned a value of $\hat{G}^s(\epsilon)$.] (48)

A second topological feature which can be identified in the $\hat{G}^m(\mathbf{k}, \epsilon)$ diagrammatic series is the node. A node is a vertex in a field circle with the following property. If the path from circle 1 to the node passes through any field circles, the path from the node to circle 2 passes through none of these circles. The path to the node must not visit circle 2 and the path from the node must not visit circle 1. Thus the node divides the circles in the diagram, except for the circle containing the node, into two uniquely defined sets, those which are visited before the node and those which are visited after the node. Circle 1 is always a member of the first set and circle 2 is always a member of the second. A diagram may contain more than one node. However we have eliminated diagrams with loops from the series, so each circle has at most one node in it. Examples of diagrams with nodes are shown in Fig. 6(A), the nodes are labeled with Greek letters.

If we compare the topological structure of diagram V in Fig. 6(A) to that of diagram VIII in Fig. 6(B) we see that diagram V looks like two segments of diagram VIII joined by merging the end vertex of the first diagram with the beginning vertex of a second diagram. The values of diagram VIII and V are

$$\mathrm{VIII}(\mathbf{k}, \epsilon) = \hat{G}^s(\epsilon)^2 \rho \int d\mathbf{r}_{12} \exp(i\mathbf{k} \cdot \mathbf{r}_{12}) w_{12} \tag{49}$$

and

$$\begin{aligned} \mathrm{V}(\mathbf{k}, \epsilon) &= \hat{G}^s(\epsilon)^3 \rho^2 \int d\mathbf{r}_{12} \exp(i\mathbf{k} \cdot \mathbf{r}_{12}) \int d\mathbf{r}_{13} w_{13} w_{32} \\ &= \hat{G}^s(\epsilon)^3 \rho^2 \left[\int d\mathbf{r}_{13} \exp(i\mathbf{k} \cdot \mathbf{r}_{13}) w_{13} \right] \\ &\quad \times \left[\int d\mathbf{r}_{32} \exp(i\mathbf{k} \cdot \mathbf{r}_{32}) w_{32} \right] . \end{aligned} \tag{50}$$

The quantities in brackets can be written in terms of $\mathrm{VIII}(\mathbf{k}, \epsilon)$ to yield

$$V(\mathbf{k}, \epsilon) = \hat{G}^s(\epsilon)^3 \rho^2 \left(\frac{\mathrm{VIII}(\mathbf{k}, \epsilon)}{\rho \hat{G}^s(\epsilon)^2} \right)^2 . \tag{51}$$

Similarly, diagram VI has the structure of two diagrams without nodes, IX and VIII, joined end to beginning. The values of IX and VI are

$$\mathrm{IX}(\mathbf{k}, \epsilon) = \hat{G}^s(\epsilon)^5 \rho^2 \int d\mathbf{r}_{12} \exp(i\mathbf{k} \cdot \mathbf{r}_{12}) \int d\mathbf{r}_{13} w_{13} w_{32} w_{21} w_{12} \tag{52}$$

and

$$\begin{aligned} \mathrm{VI}(\mathbf{k}, \epsilon) &= \hat{G}^s(\epsilon)^6 \rho^3 \int d\mathbf{r}_{12} \exp(i\mathbf{k} \cdot \mathbf{r}_{12}) \\ &\quad \times \int d\mathbf{r}_{13} \int d\mathbf{r}_{14} w_{14} w_{43} w_{31} w_{13} w_{32} \\ &= \hat{G}^s(\epsilon)^3 \rho^2 \left(\rho \hat{G}^s(\epsilon)^3 \int d\mathbf{r}_{13} \exp(i\mathbf{k} \cdot \mathbf{r}_{13}) \right. \\ &\quad \left. \times \int d\mathbf{r}_{14} w_{14} w_{43} w_{31} w_{13} \right) \left(\int d\mathbf{r}_{32} \exp(i\mathbf{k} \cdot \mathbf{r}_{32}) w_{32} \right) . \end{aligned} \tag{53}$$

Expressing $\mathrm{VI}(\mathbf{k}, \epsilon)$ in terms of $\mathrm{IX}(\mathbf{k}, \epsilon)$ and $\mathrm{VIII}(\mathbf{k}, \epsilon)$ gives

$$\mathrm{VI}(\mathbf{k}, \epsilon) = \hat{G}^s(\epsilon)^3 \rho^2 \left(\frac{\mathrm{IX}(\mathbf{k}, \epsilon)}{\rho \hat{G}^s(\epsilon)^2} \right) \left(\frac{\mathrm{VIII}(\mathbf{k}, \epsilon)}{\rho \hat{G}^s(\epsilon)^2} \right) . \tag{54}$$

This procedure is a general one. Any diagram with nodes can be constructed by joining two or more diagrams without nodes. The value of this diagram can be written in terms of the values of the diagrams used to construct it. This motivates us to define a series

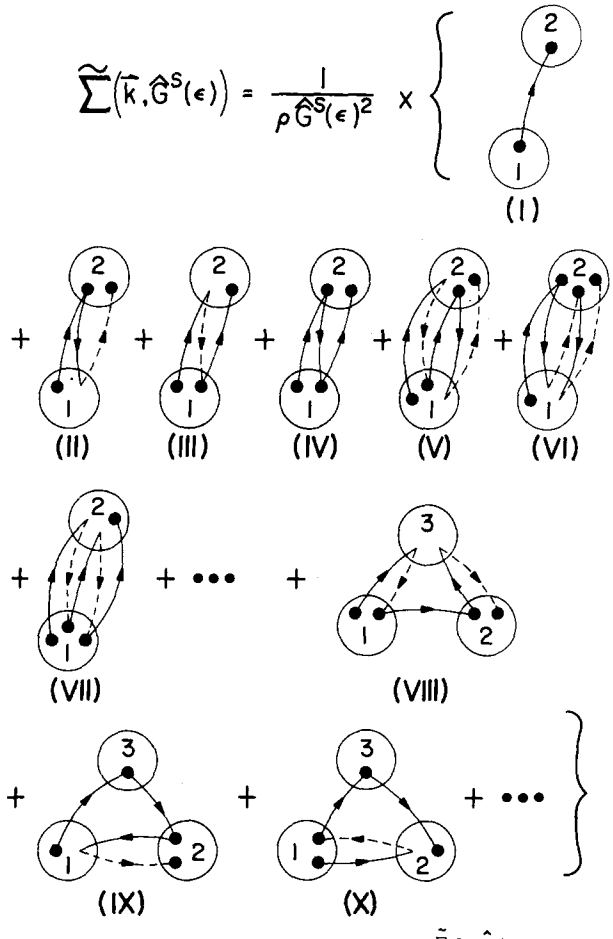

FIG. 7. The diagrammatic expansion of $\tilde{\sum}(\mathbf{k}, \hat{G}^s(\epsilon))$. Diagrams I–VII are examples of the diagrams included in the two-body approximation. All two circle diagrams and all diagrams with three circles, such as diagrams VIII–X are included in the three-body approximation.

$\sum(\mathbf{k}, \epsilon)$ by

$$\sum(\mathbf{k}, \epsilon) = \frac{1}{\rho \hat{G}^s(\epsilon)^2} \times \{\text{The sum of all diagrams in Eq. (48) for } \hat{G}^m(\mathbf{k}, \epsilon) \text{ that have no nodes.}\} \quad (55)$$

(It is easily shown that this equation is equivalent to the following one:

$$\sum(\mathbf{k}, \epsilon) = \frac{\epsilon^2}{\rho} \times \{\text{The sum of all diagrams in Eq. (42) for } \hat{G}^m(\mathbf{k}, \epsilon) \text{ that have no nodes and that have no loops on the root circles.}\} \quad (56)$$

In the following work, however, we will use Eq. (55).) It is clear from Eq. (55) that all the ϵ dependence in $\sum(\mathbf{k}, \epsilon)$ is contained in $\hat{G}^s(\epsilon)$ factors. To emphasize this we will write $\sum(\mathbf{k}, \epsilon)$ as

$$\sum(\mathbf{k}, \epsilon) = \tilde{\sum}(\mathbf{k}, \hat{G}^s(\epsilon)) . \quad (57)$$

The diagrams in $\tilde{\sum}(\mathbf{k}, \hat{G}^s(\epsilon))$ are shown in Fig. 7.

Diagrams with one node can be thought of as being constructed by joining two diagrams with no nodes. From the examples given in Eqs. (51) and (54) we expect that the value of a diagram with one node will be related to a product of two terms of the $\tilde{\sum}(\mathbf{k}, \hat{G}^s(\epsilon))$ series. If we define the sum of all diagrams in the $\hat{G}^m(\mathbf{k}, \epsilon)$ with one node as $\hat{G}_1^m(\mathbf{k}, \epsilon)$, we find that

$$\hat{G}_1^m(\mathbf{k}, \epsilon) = \rho^2 \hat{G}^s(\epsilon)^3 \left[\tilde{\sum}(\mathbf{k}, \hat{G}^s(\epsilon))\right]^2 . \quad (58)$$

A diagram with n nodes can be constructed by joining $n+1$ diagrams with no nodes. The sum of all such diagrams, $\hat{G}_n^m(\mathbf{k}, \epsilon)$, is given by

$$\hat{G}_n^m(\mathbf{k}, \epsilon) = \rho^{n+1} \hat{G}^s(\epsilon)^{n+2} \left[\tilde{\sum}(\mathbf{k}, \hat{G}^s(\epsilon))\right]^{n+1} . \quad (59)$$

$\hat{G}^m(\mathbf{k}, \epsilon)$ can be written in terms of the functions $\hat{G}_n^m(\mathbf{k}, \epsilon)$ as

$$\hat{G}^m(\mathbf{k}, \epsilon) = \sum_{n=0}^{\infty} \hat{G}_n^m(\mathbf{k}, \epsilon) = \sum_{n=0}^{\infty} \rho^{n+1} \hat{G}^s(\epsilon)^{n+2} \left[\tilde{\sum}(\mathbf{k}, \hat{G}^s(\epsilon))\right]^{n+1} . \quad (60)$$

Summing this series we get

$$\hat{G}^m(\mathbf{k}, \epsilon) = \rho \hat{G}^s(\epsilon)^2 \tilde{\sum}(\mathbf{k}, \hat{G}^s(\epsilon)) / \left[1 - \rho \hat{G}^s(\epsilon) \tilde{\sum}(\mathbf{k}, \hat{G}^s(\epsilon))\right] . \quad (61)$$

$\tilde{\sum}(\mathbf{k}, \hat{G}^s(\epsilon))$ can be interpreted as the Fourier–Laplace transform of the transfer rate for jumps which are uncorrelated with past and future jumps. An excitation visits a set of circles before the node and never returns to these circles after leaving the node. This can be represented diagrammatically by the series shown in Fig. 8. Each wavy arrow represents a factor of $\tilde{\sum}(\mathbf{k}, \hat{G}^s(\epsilon))$. A factor of $\rho \hat{G}^s(\epsilon)$ is associated with each vertex. The vertices in the field circles are nodes; a diagram with n field circles represents the sum of all diagrams in $\hat{G}^m(\mathbf{k}, \epsilon)$ with n nodes, $\hat{G}_n^m(\mathbf{k}, \epsilon)$.

We have defined $\hat{G}^s(\epsilon)$ and $\hat{G}^m(\mathbf{k}, \epsilon)$ so that the Fourier–Laplace transform of the Green function is the sum of $\hat{G}^s(\epsilon)$ and $\hat{G}^m(\mathbf{k}, \epsilon)$. Using Eq. (61) we can express $\hat{G}(\mathbf{k}, \epsilon)$ in terms of $\hat{G}^s(\epsilon)$ and $\tilde{\sum}(\mathbf{k}, \hat{G}^s(\epsilon))$

$$\hat{G}(\mathbf{k}, \epsilon) = \hat{G}^s(\epsilon) + \rho \hat{G}^s(\epsilon)^2 \tilde{\sum}(\mathbf{k}, \hat{G}^s(\epsilon)) / \left[1 - \rho \hat{G}^s(\epsilon) \tilde{\sum}(\mathbf{k}, \hat{G}^s(\epsilon))\right] = \hat{G}^s(\epsilon) \Big/ \left[1 - \rho \hat{G}^s(\epsilon) \tilde{\sum}(\mathbf{k}, \hat{G}^s(\epsilon))\right] . \quad (62)$$

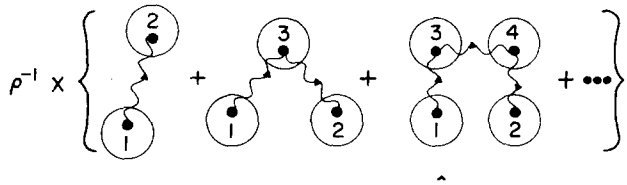

FIG. 8. The diagrammatic expansion of $\hat{G}^m(\mathbf{k}, \epsilon)$ in terms of $\tilde{\sum}(\mathbf{k}, \hat{G}^s(\epsilon))$. Each wavy arrow represents a factor of $\tilde{\sum}(\mathbf{k}, \hat{G}^s(\epsilon))$. A factor of $\rho \hat{G}^s(\epsilon)$ is associated with each vertex.

This expression can be rewritten in the form of the Green function for a generalized diffusion equation.[11] To do this we consider the $k=0$ limit of $\hat{G}(\mathbf{k},\epsilon)$. For a physically reasonable solution, i.e., one which conserves probability,

$$\lim_{k\to 0}\hat{G}(\mathbf{k},\epsilon)=\epsilon^{-1}\ . \tag{63}$$

Evaluating the expression for $\hat{G}(\mathbf{k},\epsilon)$ given by Eq. (62) at $k=0$ yields

$$\epsilon^{-1}=\hat{G}^s(\epsilon)\Big/\left[1-\rho\hat{G}^s(\epsilon)\tilde{\sum}(0,\hat{G}^s(\epsilon))\right]\ . \tag{64}$$

Solving for $\hat{G}^s(\epsilon)$, we get

$$\hat{G}^s(\epsilon)=\left[\epsilon+\rho\tilde{\sum}(0,\hat{G}^s(\epsilon))\right]^{-1}\ . \tag{65}$$

This expression is substituted for $\hat{G}^s(\epsilon)$ in Eq. (62). The result is

$$\hat{G}(\mathbf{k},\epsilon)=\left\{\epsilon+\rho\left[\tilde{\sum}(0,\hat{G}^s(\epsilon))-\tilde{\sum}(\mathbf{k},\hat{G}^s(\epsilon))\right]\right\}^{-1}\ . \tag{66}$$

If we define the generalized diffusion coefficient, $D(\mathbf{k},\epsilon)$, by

$$D(\mathbf{k},\epsilon)=(\rho/k^2)\left[\tilde{\sum}(0,\hat{G}^s(\epsilon))-\tilde{\sum}(\mathbf{k},\hat{G}^s(\epsilon))\right]\ , \tag{67}$$

the Green function has the form required for the generalized diffusion equation,[11]

$$\hat{G}(\mathbf{k},\epsilon)=[\epsilon+k^2D(\mathbf{k},\epsilon)]^{-1}\ . \tag{68}$$

The results so far are exact in the thermodynamic limit. In summary, we have introduced four important functions in the derivation of the expression for the Fourier–Laplace transform of the Green function, Eq. (68). The first of these, $\hat{G}^s(\epsilon)$, is a measure of the excitation probability on the site of initial excitation. A diagrammatic series for $\hat{G}^s(\epsilon)$ has been derived and is defined in Eq. (28). In principle $\hat{G}^s(\epsilon)$ can be calculated using this series and appropriate values for ρ and w_{ij}. The function $\hat{G}^m(\mathbf{k},\epsilon)$ is also expressed as a diagrammatic series, defined by Eq. (42). This series is re-expressed in terms of $\hat{G}^s(\epsilon)$, by removing loops, and in terms of $\tilde{\sum}(\mathbf{k},\hat{G}^s(\epsilon))$, by removing nodes, to yield the result given by Eq. (61). $\tilde{\sum}(\mathbf{k},\hat{G}^s(\epsilon))$ is defined by Eq. (55) and can be interpreted as the Fourier–Laplace transform of the time and distance dependent transfer rate for jumps which are uncorrelated with past and future jumps. In principle, $\tilde{\sum}(\mathbf{k},\hat{G}^s(\epsilon))$ can be calculated from the diagrammatic series if $\hat{G}^s(\epsilon)$, ρ, and w_{ij} are known. The final important function, $D(\mathbf{k},\epsilon)$, is defined by Eq. (67). Once the generalized diffusion coefficient is known, we can obtain the Fourier–Laplace transform of the Green function from Eq. (68).

V. COMPARISON TO OTHER WORK

Before proceeding to obtain approximations to $\tilde{\sum}(\mathbf{k},\hat{G}^s(\epsilon))$ and $\hat{G}(\mathbf{k},\epsilon)$ we will discuss the relationship of our formalism to recent work by Haan and Zwanzig[6] and by Haan.[10] As noted earlier, Haan and Zwanzig express the Green function as a density expansion. In terms of our diagrams, the nth order term in this expansion is the sum of all $\hat{G}^s(\epsilon)$ and $\hat{G}^m(\mathbf{k},\epsilon)$ diagrams with a total of $n+1$ circles. The terms corresponding to the sum of all diagrams with two circles and all diagrams with three circles were obtained exactly. Truncation of the series after the first two terms yields an approximation to the Green function which is accurate for low density and short time.

The algebraic method used by Haan is similar to the diagrammatic method we have used. The two components of the Green function are expanded in a perturbation series to yield expansions equivalent to those given in Eqs. (23) and (39). From the expansion of the function we call $\hat{G}^m(\mathbf{k},\epsilon)$ Haan identifies the algebraic equivalent of a node. The series is further simplified by a process which is equivalent to the substitution of $\hat{G}^s(\epsilon)$ factors for the ϵ^{-1} factors associated with the nodal vertices. Transport from the initial site to the final site can then be described, in terms of our diagrams, as: transport along a loop [represented by $\hat{G}^s(\epsilon)$ factor], followed by transport to the first node, transport along a loop, transport to the next node, etc. This procedure does not replace all loops by $\hat{G}^s(\epsilon)$ factors, the path between nodes will still contain loops. The function defined by Haan that describes transport between nodes is equivalent to the diagrammatic series defined by Eq. (56). Haan uses this technique to derive equations analogous to Eqs. (61), (62), and (64) which we have derived independently. The motivation for deriving these relations between $\hat{G}(\mathbf{k},\epsilon)$ and $\sum(\mathbf{k},\epsilon)$ [or $\tilde{\sum}(\mathbf{k},\hat{G}^s(\epsilon))$] can be seen in the summation of the series shown in Fig. 8 to yield Eq. (61) and is common to many problems in many-body physics.[12] An approximation to $\sum(\mathbf{k},\epsilon)$ can be used to generate an approximation to $\hat{G}(\mathbf{k},\epsilon)$ containing many of the higher order diagrams. Thus a reasonable approximation to $\sum(\mathbf{k},\epsilon)$ can, in some cases, lead to a much better approximation to $\hat{G}(\mathbf{k},\epsilon)$ than would be obtained by direct approximation of $\hat{G}(\mathbf{k},\epsilon)$. Haan, however, did not choose to use this method of approximation. Thus the powerful implications of Eqs. (61), (62), and (64) could not be exploited. The diagrammatic technique we have used removes *all* loops in the diagrams in the $\sum(\mathbf{k},\epsilon)$ series [Eq. (54)] and results in all the ϵ dependence being contained in $\hat{G}^s(\epsilon)$ factors. This form for $\tilde{\sum}(\mathbf{k},\hat{G}^s(\epsilon))$ and Eq. (65) suggest an interesting class of self-consistent approximations. This method of approximation is discussed in Sec. VI.

VI. THE SELF-CONSISTENT APPROXIMATION–APPLICATION TO THE FÖRSTER RATE

The formalism developed will be applied to the Förster rate given in Eq. (2). We will focus our attention on the transport properties of systems in which the spatial variation of the intensity of the excitation source is approximately zero over distance on the order of R_0, i.e., the small k limit. This is generally the case since the wavelength of the exciting light is much larger than R_0. For small k, the Fourier–Laplace transform of the Green function is given by

$$\hat{G}(\mathbf{k},\epsilon)=[\epsilon+k^2D(0,\epsilon)]^{-1}\ \ (\text{small } k)\,, \tag{69}$$

where

$$D(0,\epsilon)=\lim_{k\to 0}\left\{(\rho/k^2)\left[\tilde{\sum}(0,\hat{G}^s(\epsilon))-\tilde{\sum}(\mathbf{k},\hat{G}^s(\epsilon))\right]\right\}. \quad (70)$$

In addition to providing an expression for the small k limit of the Green function, calculation of $D(0,\epsilon)$ allows us to calculate the mean squared displacement of the excitation. The Laplace transform of the mean squared displacement is given exactly by

$$\langle r^2(\epsilon)\rangle=\int_0^\infty dt\exp(-\epsilon t)\langle r^2(t)\rangle$$

$$=(6/\epsilon^2)D(0,\epsilon). \quad (71)$$

The calculation of Haan and Zwanzig shows that transport is not diffusive in the short time–low density regime. A sufficient condition for diffusive transport at long times is the existence of the $\epsilon=0$ limit of $D(0,\epsilon)$. As small ϵ corresponds to long times, if the limit $D(0,0)$ exists, then at long times we have

$$\hat{G}(\mathbf{k},\epsilon)=[\epsilon+k^2D(0,0)]^{-1} \quad \text{(small } k,\epsilon). \quad (72)$$

This is the Fourier–Laplace transform of the Green function for a standard diffusion equation with diffusion constant $D(0,0)$. The mean squared displacement will increase linearly with time in this regime with a slope of $6D(0,0)$.

The method of approximation to be used here is based on a self-consistent solution for $\hat{G}^s(\epsilon)$. From Eq. (65), which will be referred to as the self-consistency equation, we see that $\hat{G}^s(\epsilon)$ can be written as a function of $\tilde{\sum}(0,\hat{G}^s(\epsilon))$. Imagine that the series for $\hat{G}^s(\epsilon)$ could be summed exactly. If this solution is substituted into the $\tilde{\sum}(\mathbf{k},\hat{G}_s(\epsilon))$ series and this series is summed exactly, evaluation of the right hand side of Eq. (65) will yield the exact solution $\hat{G}^s(\epsilon)$. There is no guarantee that arbitrary approximations for $\hat{G}^s(\epsilon)$ and $\tilde{\sum}(\mathbf{k},\hat{G}^s(\epsilon))$ will have this property. When the approximation to $\hat{G}^s(\epsilon)$ is substituted into the $\tilde{\sum}(\mathbf{k},\hat{G}^s(\epsilon))$ series and this series approximately summed, evaluation of the right-hand side of the self-consistency equation in general will not yield the original approximation to the $\hat{G}^s(\epsilon)$ series. The approximation is therefore in general not self-consistent.

To obtain a self-consistent approximation to $\hat{G}^s(\epsilon)$ the following procedure will be followed: We begin with $\hat{G}^s(\epsilon)$ as an unknown function. The diagrammatic series for $\tilde{\sum}(\mathbf{k},\hat{G}^s(\epsilon))$ is partially summed to yield an approximation to $\tilde{\sum}(\mathbf{k},\hat{G}^s(\epsilon))$ in terms of the unknown function $\hat{G}^s(\epsilon)$. Substitution of this approximation for $\tilde{\sum}(\mathbf{k},\hat{G}^s(\epsilon))$ into the self-consistency equation results in an equation, involving $\hat{G}^s(\epsilon)$ and ϵ, which can be solved for the self-consistent solution for $\hat{G}^s(\epsilon)$. This solution is then substituted into $\tilde{\sum}(\mathbf{k},\hat{G}^s(\epsilon))$ to give the corresponding approximation to $\tilde{\sum}(\mathbf{k},\hat{G}^s(\epsilon))$. This procedure does not directly use the diagrammatic series for $\hat{G}^s(\epsilon)$; instead it relies on Eq. (65) to obtain $\hat{G}^s(\epsilon)$ from an approximation for $\tilde{\sum}(\mathbf{k},\hat{G}^s(\epsilon))$.

The diagrammatic series for $\tilde{\sum}(\mathbf{k},\hat{G}^s(\epsilon))$, defined by Eq. (55), is shown in Fig. 7. The diagrams in the series can be grouped according to the number of circles in the diagram. If we do this $\tilde{\sum}(\mathbf{k},\hat{G}^s(\epsilon))$ can be written as

$$\tilde{\sum}(\mathbf{k},\hat{G}^s(\epsilon))=\sum_{n=2}^{\infty}\tilde{\sum}_n(\mathbf{k},\hat{G}^s(\epsilon)), \quad (73)$$

where

$$\tilde{\sum}_n(\mathbf{k},\hat{G}^s(\epsilon))=\frac{1}{\rho\hat{G}^s(\epsilon)^2}\times\{\text{the sum of all diagrams in } \tilde{\sum}(\mathbf{k},\hat{G}^s(\epsilon)) \text{ with a total of } n \text{ circles}\}. \quad (74)$$

$\tilde{\sum}_n(\mathbf{k},\hat{G}^s(\epsilon))$ will be referred to as the n-body term. The first approximation to this series is

$$\tilde{\sum}(\mathbf{k},\hat{G}^s(\epsilon))=\tilde{\sum}_2(\mathbf{k},\hat{G}^s(\epsilon)). \quad (75)$$

Diagrams I–VII in Fig. 7 are examples of diagrams included in the two-body term. *This approximation should not be confused with the first order term of a density expansion. The presence of a $\hat{G}^s(\epsilon)$ factor for each vertex generates loops at the vertices, thus each diagram includes many higher order contributions.*

To sum $\tilde{\sum}_2(\mathbf{k},\hat{G}^s(\epsilon))$, the diagrams will be grouped according to their order, i.e., the number of solid arrows in the diagram. The nth order diagrams will be summed to yield functions denoted by $\tilde{\sum}_2^n(\mathbf{k},\hat{G}^s(\epsilon))$ so that

$$\tilde{\sum}_2(\mathbf{k},\hat{G}^s(\epsilon))=1/(\rho\hat{G}^s(\epsilon)^2)\sum_{n=1}^{\infty}\tilde{\sum}_2^n(\mathbf{k},\hat{G}^s(\epsilon)). \quad (76)$$

There is only one first order diagram, diagram (I) in Fig. 7, so $\tilde{\sum}_2^1(\mathbf{k},\hat{G}^s(\epsilon))$ is equal to the value of this diagram

$$\tilde{\sum}_2^1(\mathbf{k},\hat{G}^s(\epsilon))=\rho\hat{G}^s(\epsilon)^2\int d\mathbf{r}_{12}\exp(i\mathbf{k}\cdot\mathbf{r}_{12})w_{12}. \quad (77)$$

The two second order diagrams, diagrams (II) and (III) in Fig. 7, are equal in value. Summing these diagrams we have

$$\tilde{\sum}_2^2(\mathbf{k},\hat{G}^s(\epsilon))=-2\rho\hat{G}^s(\epsilon)^3\int d\mathbf{r}_{12}\exp(i\mathbf{k}\cdot\mathbf{r}_{12})w_{12}^2. \quad (78)$$

The four third order diagrams, diagrams (IV)–(VII) in Fig. 7, are also all equal and when summed give

$$\tilde{\sum}_2^3(\mathbf{k},\hat{G}^s(\epsilon))=4\rho\hat{G}^s(\epsilon)^4\int d\mathbf{r}_{12}\exp(i\mathbf{k}\cdot\mathbf{r}_{12})w_{12}^3. \quad (79)$$

These terms appear to be the leading terms in a geometric series. To prove this we need to calculate the general term, $\tilde{\sum}_2^n(\mathbf{k},\hat{G}^s(\epsilon))$. We first note that every diagram in the series contains an odd number of arrows. For n odd, the diagram contains an odd number of solid arrows and thus must contain an even number of dashed arrows. The product of -1 factors associated with the dashed arrows is therefore equal to $+1$. Similarly, for n even the product of -1 factors results in a net factor of -1. Each nth order diagram will therefore have the value

$$\rho\hat{G}^s(\epsilon)^{n+1}(-1)^{n+1}\int d\mathbf{r}_{12}\exp(i\mathbf{k}\cdot\mathbf{r}_{12})w_{12}^n. \quad (80)$$

We now need to determine the number of nth order diagrams. The presence of only two circles in all diagrams considerably simplifies this problem. The diagram

may begin in two ways, with a solid arrow to circle 2 or with a solid arrow to circle 2 followed by dashed arrow back to circle 1. For each of these cases there are two ways to continue the diagram, either with a solid arrow to the other circle or with a solid arrow to the other circle and a dashed arrow back. This procedure can be carried out $n-1$ times, there will always be two ways to continue each diagram. For each of these 2^{n-1} partial diagrams there is only one way to end the diagram. The path of arrows must end on circle 2. Therefore if the end point of the path is on circle 1 after $n-1$ steps the diagram must end with a solid arrow to circle 2. If the end point of the path is on circle 2 after $n-1$ steps the diagram must end with a solid arrow to circle 1 followed by a dashed arrow back to 2. Thus there are a total of 2^{n-1} nth order diagrams, each of which has the value given by (80) so that

$$\tilde{\sum}_2^n(\mathbf{k}, \hat{G}^s(\epsilon)) = \rho \hat{G}^s(\epsilon)^{n+1}(-2)^{n-1}\int d\mathbf{r}_{12}\exp(i\mathbf{k}\cdot\mathbf{r}_{12})w_{12}^n\,, \quad (81)$$

and

$$\tilde{\sum}_2(\mathbf{k}, \hat{G}^s(\epsilon)) = \int d\mathbf{r}_{12}\exp(i\mathbf{k}\cdot\mathbf{r}_{12})\left[\sum_{n=1}^{\infty}\hat{G}^s(\epsilon)^{n-1}(-2)^{n-1}w_{12}^n\right]. \quad (82)$$

Summing the series we obtain

$$\tilde{\sum}_2(\mathbf{k}, \hat{G}^s(\epsilon)) = \int d\mathbf{r}_{12}\exp(i\mathbf{k}\cdot\mathbf{r})\left(\frac{w_{12}}{1+2\hat{G}^s(\epsilon)w_{12}}\right). \quad (83)$$

It should be noted that although w_{12} may diverge for small r_{12}, the quantity in brackets is finite for all r_{12}.

Evaluating the expression in Eq. (83) at $k=0$ gives

$$\tilde{\sum}_2(0, \hat{G}^s(\epsilon)) = \int d\mathbf{r}_{12}\frac{w_{12}}{1+2\hat{G}^s(\epsilon)w_{12}} \quad (84)$$

so the self-consistency equation for the two-body approximation to $\hat{G}^s(\epsilon)$ is

$$\hat{G}^s(\epsilon) = \left(\epsilon + \rho\int d\mathbf{r}_{12}\frac{w_{12}}{1+2\hat{G}^s(\epsilon)w_{12}}\right)^{-1}. \quad (85)$$

Substituting the Förster rate yields

$$\hat{G}^s(\epsilon) = \left(\epsilon + \frac{4\pi\rho}{\tau}\int_0^{\infty} dr_{12}\frac{(R_0/r_{12})^6}{1+(2\hat{G}^s(\epsilon)/\tau)(R_0/r_{12})^6}\right)^{-1}. \quad (86)$$

For a physically reasonable solution, $\hat{G}^s(\epsilon)$ is a positive real number for ϵ on the positive real axis. For this case the integral can be analytically evaluated to give

$$\hat{G}^s(\epsilon) = \left[\epsilon + \frac{\pi C}{2\tau}\left(\frac{\tau}{2\hat{G}^s(\epsilon)}\right)^{1/2}\right]^{-1}, \quad (87)$$

where the dimensionless concentration C is defined by

$$C = (4\pi R_0^3/3)\rho\,. \quad (88)$$

$\hat{G}^s(\epsilon)^{1/2}$ is to be interpreted as the positive square root of $\hat{G}^s(\epsilon)$. Equation (87) is a quadratic equation in $\hat{G}^s(\epsilon)^{1/2}$,

$$\epsilon\hat{G}^s(\epsilon) + [\pi C/(2^{3/2}\tau^{1/2})]\hat{G}^s(\epsilon)^{1/2} - 1 = 0\,. \quad (89)$$

$\hat{G}^s(\epsilon)^{1/2}$ must be a positive real number so we have the following unique solution

$$\hat{G}^s(\epsilon)^{1/2} = \left[-\frac{\pi C\tau^{1/2}}{2^{3/2}} + \left(\frac{\pi^2C^2\tau}{8} + 4\epsilon\tau\right)^{1/2}\right]\Big/ 2\epsilon\tau \quad (90)$$

and

$$\hat{G}^s(\epsilon) = \left\{\frac{\pi^2C^2}{4}\left[1-\left[1+\frac{32\epsilon\tau}{\pi^2C^2}\right]^{1/2}\right] + 4\epsilon\tau\right\}\Big/ 4\epsilon^2\tau\,. \quad (91)$$

In the derivation of the solution given by Eq. (91) we have assumed that ϵ is on the positive real axis. However this solution can be analytically continued to the right half-plane to yield a well defined transform.

To obtain expressions for the small k limit of the Green function and the mean squared displacement we need to calculate the $k=0$ limit of the generalized diffusion coefficient. Substitution of the two-body approximation to $\tilde{\sum}(\mathbf{k}, \hat{G}^s(\epsilon))$ into Eq. (67) yields

$$D(\mathbf{k}, \epsilon) = \frac{\rho}{k^2}\int d\mathbf{r}_{12}[1-\exp(i\mathbf{k}\cdot\mathbf{r}_{12})]\left[\frac{w_{12}}{1+2\hat{G}^s(\epsilon)w_{12}}\right]$$
$$= \frac{\rho}{k^2}\int d\mathbf{r}_{12}\left[1-\frac{\sin(kr_{12})}{kr_{12}}\right]\left[\frac{w_{12}}{1+2\hat{G}^s(\epsilon)w_{12}}\right]. \quad (92)$$

Taking the limit as $k\to 0$ we get

$$D(0, \epsilon) = \frac{\rho}{6}\int d\mathbf{r}_{12}\frac{r_{12}^2 w_{12}}{1+2\hat{G}^s(\epsilon)w_{12}}\,. \quad (93)$$

Substituting the Förster rate we have

$$D(0, \epsilon) = \frac{\rho R_0^6}{6\tau}\int d\mathbf{r}_{12}\frac{r_{12}^{-4}}{1+(2\hat{G}^s(\epsilon)/\tau)(R_0/r_{12})^6}$$
$$= \frac{CR_0^2}{6\tau}\int_0^{\infty} dx\frac{x^{2/3}}{x^2+2\hat{G}^s(\epsilon)/\tau}\,. \quad (94)$$

The integration is performed analytically to yield

$$D(0, \epsilon) = (\pi CR_0^2\tau^{-1}/6)(2\hat{G}^s(\epsilon)/\tau)^{-1/6}\,, \quad (95)$$

where $\hat{G}^s(\epsilon)$ is given by Eq. (91). Substitution of this expression into Eqs. (69) and (71) yields expressions for the small k limit of the Green function and the Laplace transform of the mean squared displacement.

For long time diffusive transport the limit as $\epsilon\to 0$ of $D(0, \epsilon)$ must exist. This limit will exist since $\hat{G}^s(\epsilon)$ approaches a nonzero limit as $\epsilon\to 0$. Taking the $\epsilon\to 0$ limit of Eq. (91) we have

$$\hat{G}^s(0) = 8\tau/(\pi^2C^2) \quad (96)$$

and therefore

$$D(0, 0) = 0.483\,C^{4/3}R_0^2\tau^{-1}\,. \quad (97)$$

The form of the diffusion constant is the same as that found by Förster for transport on a periodic lattice. The value of the coefficient in his expression depends somewhat on the type of lattice. For a simple cubic lattice the value is 0.409.[6(a)]

At this point there is no guarantee that this approximation is accurate for the Förster rate. The diagrams summed in obtaining it include all diagrams which are first order in C, i.e., those diagrams summed in Haan and Zwanzig's first order result, *plus many higher order diagrams*. Thus our approximation will be valid in the short time–low density regime. It is not obvious from our expressions for $\hat{G}^s(\epsilon)$ and $D(0, \epsilon)$ that the short time (large ϵ) behavior is the same as that found by Haan and Zwanzig. If we expand $\hat{G}^s(\epsilon)$ as a series in decreasing powers of ϵ we find

$$\hat{G}^s(\epsilon) = \epsilon^{-1} - (\pi\sqrt{2}C)/(4\tau^{1/2}\epsilon^{-3/2}) + 0(\epsilon^{-2})\,. \quad (98)$$

Substitution of this expression into Eq. (95) yields

$$D(0,\epsilon) = 0.4665 C R_0^2 \epsilon^{1/6} \tau^{-5/6} + 0.08635 C^2 R_0^2 \epsilon^{-1/3} \tau^{-4/3} + 0(\epsilon^{-5/6}) . \quad (99)$$

This power series has the form demanded by the scaling law.[8] Using Eq. (71) we can write $\langle r^2(\epsilon)\rangle$ as a power series in ϵ

$$\langle r^2(\epsilon)\rangle = 2.799 C R_0^2 \epsilon^{-11/6} \tau^{-5/6} + 0.5181 C^2 R_0^2 \epsilon^{-7/3} \tau^{-4/3} + 0(\epsilon^{-17/6}) . \quad (100)$$

This series can be inverted term by term to give

$$\langle r^2(t)\rangle / R_0^2 = 2.975 C (t/\tau)^{5/6} + 0.4352 C^2 (t/\tau)^{4/3} + 0(t^{11/6}) . \quad (101)$$

As expected from the diagrams summed, the term linear in C is the same as Haan and Zwanzig's result. The coefficient of the second order term is 33% larger than Haan and Zwanzig's result.

To estimate the accuracy of our solution in the long time–high density regime, the second approximation to $\tilde{\sum}(\mathbf{k}, \hat{G}^s(\epsilon))$ has been obtained and the self-consistency equation solved to give a second approximation to $\hat{G}^s(\epsilon)$. The second approximation to $\tilde{\sum}(\mathbf{k}, \hat{G}^s(\epsilon))$ is the sum of all diagrams in the series with three circles or fewer,

$$\tilde{\sum}(\mathbf{k}, \hat{G}^s(\epsilon)) = \tilde{\sum}_2(\mathbf{k}, \hat{G}^s(\epsilon)) + \tilde{\sum}_3(\mathbf{k}, \hat{G}^s(\epsilon)) . \quad (102)$$

The first approximation was relatively straightforward to calculate as there is no way to construct a $\hat{G}^m(\mathbf{k}, \epsilon)$ diagram with two circles that contains a loop or node. Thus we summed all diagrams with two circles. Diagrams with three circles containing a loop or node can be constructed, so the summation procedure is much more involved. The details of the calculations needed to obtain the three-body approximation are included in the Appendix. The results are

$$\tilde{\sum}_3(\mathbf{k}, \hat{G}^s(\epsilon)) = \rho^{-1} \hat{G}^s(\epsilon)^{-2} [\tilde{A}_3(\mathbf{k}, \hat{G}^s(\epsilon)) - \tilde{L}_3(\mathbf{k}, \hat{G}^s(\epsilon)) - \tilde{N}_3(\mathbf{k}, \hat{G}^s(\epsilon))], \quad (103)$$

where

$$\tilde{A}_3(\mathbf{k}, \hat{G}^s(\epsilon)) = \hat{G}^s(\epsilon)\rho^2 \int d\mathbf{r}_{12} \exp(i\mathbf{k}\cdot\mathbf{r}_{12}) \int d\mathbf{r}_{12} \left[\frac{\hat{G}^s(\epsilon)^{-1} w_{12} + w_{12}w_{13} + w_{12}w_{23} + w_{13}w_{23}}{\hat{G}^s(\epsilon)^{-2} + 2\hat{G}^s(\epsilon)^{-1}(w_{12}+w_{13}+w_{23}) + 3(w_{12}w_{13} + w_{12}w_{23} + w_{13}w_{23})} - \frac{w_{12}}{\hat{G}^s(\epsilon)^{-1} + 2w_{12}} \right], \quad (104)$$

$$\tilde{L}_3(\mathbf{k}, \hat{G}^s(\epsilon)) = -\frac{2^{3/2}\pi^2 R_0^3 \rho^2 \hat{G}^s(\epsilon)^{5/2}}{3\tau^{1/2}} \int d\mathbf{r}_{12} \exp(i\mathbf{k}\cdot\mathbf{r}_{12}) \times \frac{w_{12}(1+\hat{G}^s(\epsilon)w_{12})}{(1+2\hat{G}^s(\epsilon)w_{12})^2} , \quad (105)$$

and

$$\tilde{N}_3(\mathbf{k}, \hat{G}^s(\epsilon)) = \rho^2 \hat{G}^s(\epsilon)^3 \int d\mathbf{r}_{12} \exp(i\mathbf{k}\cdot\mathbf{r}_{12}) \int d\mathbf{r}_{13} \times \left(\frac{w_{13}}{1+2\hat{G}^s(\epsilon)w_{13}}\right)\left(\frac{w_{32}}{1+2\hat{G}^s(\epsilon)w_{32}}\right) . \quad (106)$$

Solution of the self-consistency equation yields

$$\hat{G}^s(\epsilon) = \tau \left\{ \frac{\pi^2 C^2}{4} \left[1 - \left[1 + \frac{32}{\pi^2 C^2} (\epsilon\tau - 0.18870 C^2) \right]^{1/2} \right] + 4(\epsilon\tau - 0.18870 C^2) \right\} \Big/ [4(\epsilon\tau - 0.18870 C^2)^2] . \quad (107)$$

The second approximation to the $k=0$ limit of the generalized diffusion coefficient is

$$D(0,\epsilon) = (\pi C R_0^2 \tau^{-1}/6)(2\hat{G}^s(\epsilon)/\tau)^{-1/6} - 0.02145 C^2 R_0^2 \hat{G}^s(\epsilon)^{1/3} \tau^{-4/3} . \quad (108)$$

Taking the $\epsilon = 0$ limit we obtain

$$D(0,0) = 0.428 C^{4/3} R_0^2 \tau^{-1} . \quad (109)$$

These results do not constitute a proof that the long time motion is diffusive for this model. However, they strongly suggest that this is the case and that Eq. (109) is a good approximation to the correct diffusion constant. Incidentally, by a scaling principle analysis, Haan and Zwanzig proved that if the motion is diffusive for this model, the diffusion coefficient must be a pure number times $C^{4/3} R_0^2/\tau$. Both Eqs. (109) and (97) are consistent with this result.

VII. RESULTS

Even if transport is diffusive for long times and high density, it is important to know the mode of transport for times of experimental interest, i.e., $t \lesssim 2\tau$. As the excited state population is decaying exponentially with lifetime τ, transport at times greater than a few τ is not important. To examine transport for times of experimental interest we will calculate the mean squared displacement, $\langle r^2(t)\rangle$. The Laplace transform of the mean squared displacement is given by Eq. (71). The two- and three-body approximations to $D(0,\epsilon)$ are substituted into this expression which is then numerically inverted by the method of Stehfest[13] to give $\langle r^2(t)\rangle$. The results of this calculation are shown in Fig. 9. For diffusive transport $\langle r^2(t)\rangle$ increases linearly with time with slope $6D(0,0)$. The derivative of $\langle r^2(t)\rangle$ was calculated numerically for the curves shown in Fig. 9, to give the results shown in Fig. 10. For low concentrations such as $C = 0.1$, which is shown in Figs. 9(A) and 10(A), transport is not diffusive for $t < 2.5\tau$. The transport for this case is well described by Haan and Zwanzig's approximation to the density expansion. Their second order approximation is indistinguishable from the three-body self-consistent approximation for the range of times calculated. For extremely long times the self-consistent solutions will become diffusive, i.e., the slope will become equal to the constant value indicated by the horizontal line in Fig. 10(A). For inter-

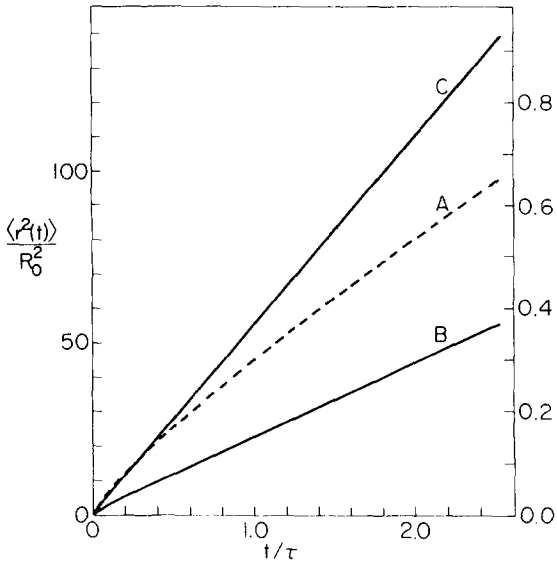

FIG. 9. The mean squared displacement of the excitation for $C = 0.1$ (A), $C = 5.0$ (B), and $C = 10.0$ (C). The results shown were calculated with the three body approximations to $D(0, \epsilon)$ [Eq. (108)] and $\hat{G}^s(\epsilon)$ [Eq. (107)]. The left vertical scale is for curves (B) and (C); the right vertical scale is for curve (A). Time is in units of the excited state lifetime, τ.

mediate concentrations such as $C = 5.0$, shown in Figs. 9(B) and 10(B), transport is nondiffusive for $t \lesssim \tau$ and diffusive for $t \gtrsim \tau$. For comparison these results are shown with Haan and Zwanzig's result for $C = 5.0$ in Fig. 11. For high concentrations such as $C = 10.0$ which is shown in Figs. 10(C) and 11(C), transport becomes diffusive in a small fraction of the excited state lifetime. For very large concentrations transport is diffusive for essentially all times.

VIII. EXPERIMENTAL OBSERVABLES—PICOSECOND TRANSIENT GRATING TECHNIQUE

To verify the model an experimental observable related to one of the functions calculated is needed. The necessary observable is provided in the picosecond transient grating experiment.[2(b),9] In this experiment a delayed picosecond probe pulse is Bragg diffracted by a grating which is optically produced in the sample by the interference of two coherent picosecond excitation pulses. Absorption by the sample in the overlap region of the two excitation pulses results in a spatially varying sinusoidal distribution of excited states. The probe pulse encounters a sinusoidal spatial variation in the complex index of refraction and Bragg diffraction results. The intensity of the diffracted probe pulse is proportional to the square of the difference in absorption between the grating peaks and nulls. Time dependent processes which reduce this peak–null difference result in the decay of the diffracted signal.

The transient grating method can be applied to the study of Förster transfer in random systems in two ways. We first consider low concentration systems. To eliminate the effects of molecular rotation the experiment would be done in a viscous solvent such as glycerol or in a glass. In the low concentration regime the long range transfer of excitations from the peak regions to null regions is negligible. The peak–null spacing, which is dependent on the excitation wavelength and the angle between the excitation beams, is much greater than the mean squared displacement for all times for which the excited state population has not decayed by lifetime processes. Although long range transport will not affect the diffracted intensity, effects of energy transfer will still be measurable through the state of polarization. As the sample is initially excited with polarized excitation pulses, molecules having their transition dipole parallel to the excitation polarization will be preferentially excited. For the case where the probe pulse has the same polarization and wavelength as the excitation pulses and there is no excited state–excited state absorption, the probe pulse sees a distribution of transition dipoles with a portion of aligned dipoles removed. Thus in addition to fewer ground states avail-

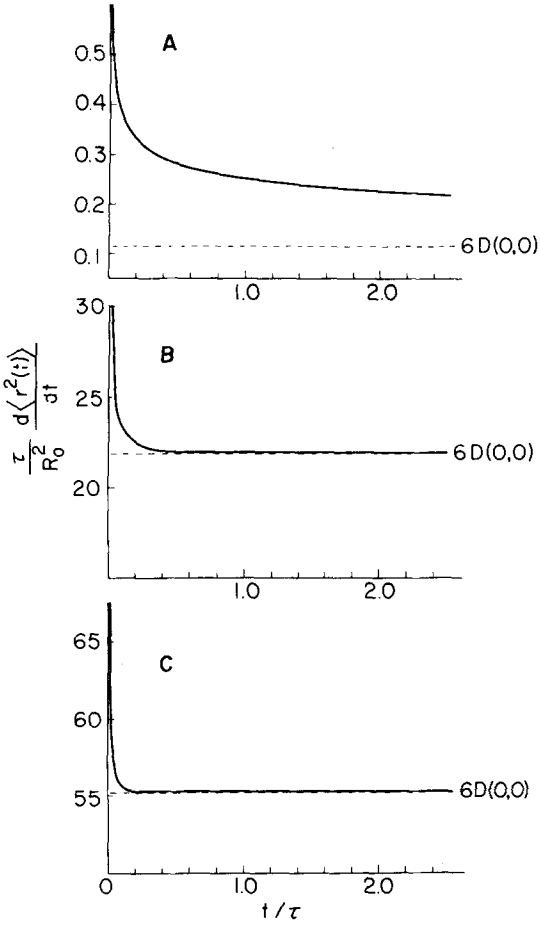

FIG. 10. The time derivative of the mean squared displacement for $C = 0.1$ (A), $C = 5.0$ (B), and $C = 10.0$ (C). The curves were calculated numerically from the results shown in Fig. 9. The constant slope 6 $D(0, 0)$ associated with diffusive transport is shown by a dashed horizontal line in each plot. For $C = 0.1$, transport is nondiffusive for all times calculated. At extremely long time transport will be diffusive. However, this will require many excited state lifetimes. Thus for practical purposes, transport is nondiffusive. For $C = 5.0$, transport is diffusive for $t \geq \tau$; for $C = 10.0$, transport is diffusive for $t \geq 0.3\,\tau$. The corresponding two-body approximation results (not shown) are only slightly different, see Fig. 11.

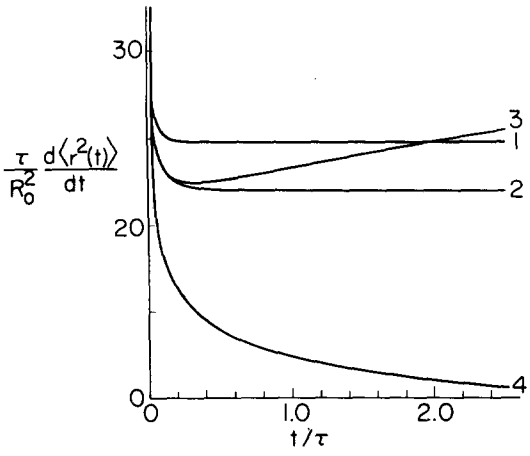

FIG. 11. The time derivative of the mean squared displacement is shown for $C = 5.0$. The two-body (1) and three-body (2) self-consistent results obtained in this paper are compared to the first order (4) and second order (3) density expansion results obtained by Haan and Zwanzig. Only a small change is seen between the self-consistent results, the diffusion constant is ~10% smaller for the three-body result and transport becomes diffusive somewhat later. The first order and second order density expansion results are considerably different and neither result shows diffusive behavior.

able to absorb the probe at the peaks, the effective cross section at the peaks will also be smaller. Calculations of the fluorescence depolarization due to Förster transfer indicate that most of the polarization retained by the system is due to excitations at the initial sites.[4] As excitation transfer occurs the distribution of excited dipoles randomizes, i.e., the excitation is transferred to a dipole of approximately random orientation. In the transient grating experiment this leads to a return to a random distribution of dipole orientations for the unexcited molecules at the grating peaks at long times and to a decrease in the difference in cross section between peak and null to zero. For the model developed here the probability that the excitation is at the site of initial excitation at time t is $G^s(t)$. If we make the approximation that excitation transfer is to a completely random dipole the diffracted probe intensity, $I_D(t)$, for this type of experiment will be given by

$$I_D(t) \propto (1 + 0.8G^s(t))^2 . \tag{110}$$

$\hat{G}^s(\epsilon)$ has been numerically inverted with the Stehfest method[13] and is shown in Fig. 12. For the concentrations shown in Fig. 12, $G^s(t)$ decays appreciably over times accessible to study with the picosecond grating technique.[9]

In some respects this experiment is similar to the method used by Eisenthal and co-workers[14] to study rotational relaxation. In this experiment the sample is excited with a polarized picosecond excitation pulse. The orientation of the unexcited dipoles is no longer random after excitation, molecules with dipoles aligned with the excitation polarization are preferentially excited. The transmission of a delayed probe pulse is thus greater than would be found for a random distribution of dipoles. The important difference between the two techniques lies in the fact that the diffracted signal depends on the difference in absorption between peak and null and, as the signal is detected against a dark background, this difference need not be large. To detect changes in the transmission in the probe pulse experiment the ground state must be depleted considerably, i.e., the sample is bleached or saturated.

In the extreme high concentration limit the mean squared displacement of the excitation is comparable to the peak–null spacing of the grating and therefore long range transport will contribute to the decay of the transient grating signal. $G^s(t)$ decays to zero essentially immediately for high concentrations. All polarization is immediately lost and any decay of the signal after the initial rapid decrease due to depolarization will be due to a decrease in the excited state density difference between the peaks and nulls. The initial condition for the experiment can be written as

$$F(x) \propto \cos(k_G x) + 1 , \tag{111}$$

where x is a distance along the length of the grating and k_G is the grating wave vector. The Laplace transform of the peak–null difference, $\tilde{P}(\epsilon; k_G)$ will be given by

$$\tilde{P}(\epsilon; k_G) \propto \hat{G}(k_G, \epsilon) . \tag{112}$$

For high concentration systems transport is diffusive for all reasonable times. Thus the peak–null difference will decay as $\exp(-k_G^2 D(0,0)t)$. When $k_G^2 D(0,0)$ is comparable to τ^{-1} the transient grating technique can be

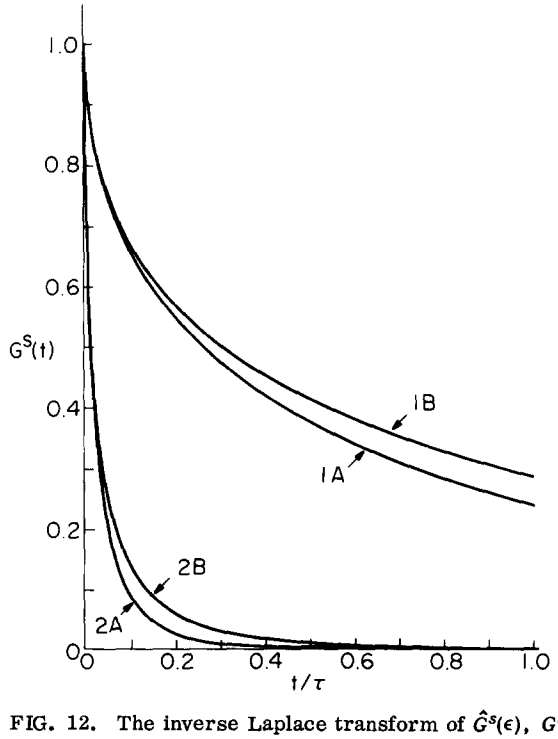

FIG. 12. The inverse Laplace transform of $\hat{G}^s(\epsilon)$, $G^s(t)$. Curve 1A is the two-body self-consistent approximation, $C = 1.0$. Curve 1B is the three-body self-consistent approximation, $C = 1.0$. Curve 2A is the two-body approximation, $C = 5.0$. Curve 2B is the three-body approximation, $C = 5.0$. $G^s(t)$ is the probability of finding the excitation on the initial site and is related to an experimental observable, the time decay of a transient grating signal in the low concentration regime.

used to directly measure $D(0,0)$. Before experimentally testing the model, the calculations presented here will have to be modified to include the complete Förster rate with orientation factors. This result and experimental results from the transient grating technique will be discussed in a subsequent publication.[9]

IX. SUMMARY

A model has been developed to describe the transport of electronic excitations in solutions. The Green function solution was written as a diagrammatic series for which a self-consistent solution is derived. The approximation includes many high order diagrams and is well-behaved in the long time-high density regime as well as in the short time-low density regime. The results of the approximation indicate that transport by the Förster mechanism is not diffusive at short times and diffusive for sufficiently long times. This is the first comprehensive treatment of Förster transfer in solution. The application of the picosecond transient grating technique to the study of excitation transport in random systems was discussed.

The theoretical technique developed here may be applicable to a number of related problems. The transport of excitations in mixed crystals could be modeled by the replacement of the integration over spatial position with a sum over lattice sites.[15] Such a study would be of interest in relation to percolation problems.[2(a)] The application of this technique to the study of trapping may also yield interesting results.[2(c)]

ACKNOWLEDGMENTS

We would like to thank S. W. Haan for providing a copy of his thesis. This work was supported by the National Science Foundation, Division of Materials Research grant DMR 76-22019. In addition, acknowledgment is made to the Donors of the Petroleum Research Fund, administered by the American Chemical Society, for partial support of this research.

APPENDIX A: CALCULATION OF THE THREE-BODY APPROXIMATIONS

To obtain $\tilde{\Sigma}_3(\mathbf{k}, \hat{G}^s(\epsilon))$ we must sum all diagrams in $\hat{G}^m(\mathbf{k}, \epsilon)$ with three circles and no nodes or loops. Diagrams VIII–X in Fig. 7 are examples of the diagrams to be summed. The simplest way to do this is to use the original diagrammatic series for $\hat{G}^m(\mathbf{k}, \epsilon)$, defined by Eq. (42). The three-body term is obtained by summing all diagrams with three circles and then subtracting the sum of all diagrams with three circles that contain a loop and the sum of all diagrams with three circles that contain a node. If the substitution of $\hat{G}^s(\epsilon)$ for ϵ^{-1} is then made in each of these sums, the three-body term will be given by

$$\tilde{\Sigma}_3(\mathbf{k}, \hat{G}^s(\epsilon)) = \rho^{-1}\hat{G}^s(\epsilon)^{-2} \times [\tilde{A}_3(\mathbf{k}, \hat{G}^s(\epsilon)) - \tilde{L}_3(\mathbf{k}, \hat{G}^s(\epsilon)) - N_3(\mathbf{k}, \hat{G}^s(\epsilon))], \tag{A1}$$

where

$\tilde{A}_3(\mathbf{k}, \hat{G}^s(\epsilon))$ = the sum of all diagrams in $\hat{G}^m(\mathbf{k}, \epsilon)$ [Eq. (42)] with three circles, (A2)

$\tilde{L}_3(\mathbf{k}, \hat{G}^s(\epsilon))$ = the sum of all diagrams in $\hat{G}^m(\mathbf{k}, \epsilon)$ [Eq. (42)] with three circles that contain a loop, (A3)

and

$\tilde{N}_3(\mathbf{k}, \hat{G}^s(\epsilon))$ = the sum of all diagrams in $\hat{G}^m(\mathbf{k}, \epsilon)$ [Eq. (42)] with three circles that contain a node. (A4)

The dependence of each of these functions on $\hat{G}^s(\epsilon)$ is due to the implied substitution of $\hat{G}^s(\epsilon)$ for ϵ^{-1}.

The first step is to obtain $\tilde{A}_3(\mathbf{k}, \hat{G}^s(\epsilon))$. We write $\hat{G}^m(\mathbf{k}, \epsilon)$ as a density expansion (following Haan and Zwanzig[8])

finite volume, Ω

$$\hat{G}^m(\mathbf{k}, \epsilon) = \frac{N-1}{\Omega} B_2^m(\mathbf{k}, \epsilon, \Omega) + \frac{(N-1)(N-2)}{\Omega^2} B_3^m(\mathbf{k}, \epsilon, \Omega) + \cdots, \tag{A5}$$

thermodynamic limit

$$\hat{G}^m(\mathbf{k}, \epsilon) = \rho B_2^m(\mathbf{k}, \epsilon) + \rho^2 B_3^m(\mathbf{k}, \epsilon) + \cdots, \tag{A6}$$

where

$$B_n^m(\mathbf{k}, \epsilon) = \lim_{\Omega \to \infty} B_n^m(\mathbf{k}, \epsilon, \Omega). \tag{A7}$$

The term $\rho^2 B_3^m(\mathbf{k}, \epsilon)$ is the sum of all diagrams with two circles in the thermodynamic limit. The coefficient $B_3^m(\mathbf{k}, \epsilon)$ is obtained from the exact solutions of the finite volume two and three particle systems. For $N=3$, Eq. (20) becomes

$$\hat{G}^m(\mathbf{k}, \epsilon) = 2\langle \exp(i\mathbf{k}\cdot\mathbf{r}_{12})[(\epsilon - \mathbf{W})^{-1}]_{12}\rangle. \tag{A8}$$

Setting this equal to the density expansion we get

$$B_3^m(\mathbf{k}, \epsilon, \Omega) = \Omega^2\langle \exp(i\mathbf{k}\cdot\mathbf{r}_{12})[(\epsilon - \mathbf{W})^{-1}]_{12}\rangle - \Omega B_2^m(\mathbf{k}, \epsilon, \Omega). \tag{A9}$$

$B_2^m(\mathbf{k}, \epsilon, \Omega)$ is obtained from the exact solution of the finite volume two particle problem,

$$B_2^m(\mathbf{k}, \epsilon, \Omega) = \int_\Omega d\mathbf{r}_{12} \exp(i\mathbf{k}\cdot\mathbf{r}_{12}) \frac{w_{12}}{\epsilon(\epsilon + 2w_{12})}. \tag{A10}$$

Substituting back into Eq. (A9) we get

$$B_3^m(\mathbf{k}, \epsilon, \Omega) = \int d\mathbf{r}_{12} \exp(i\mathbf{k}\cdot\mathbf{r}_{12}) \int d\mathbf{r}_{13} \times \left\{ [(\epsilon - \mathbf{W})^{-1}]_{12} - \frac{w_{12}}{\epsilon(\epsilon + 2w_{12})} \right\}. \tag{A11}$$

For the three particle system $\epsilon - \mathbf{W}$ is easily inverted to give

$$[(\epsilon - \mathbf{W})^{-1}]_{12} = \frac{\epsilon w_{12} + w_{12}w_{13} + w_{12}w_{23} + w_{13}w_{23}}{\epsilon[\epsilon^2 + 2\epsilon(w_{12} + w_{13} + w_{23}) + 3(w_{12}w_{13} + w_{12}w_{23} + w_{13}w_{23})]}. \tag{A12}$$

$B_3^m(\mathbf{k}, \epsilon)$ is obtained from Eq. (A11) by letting Ω go to infinity. To get $\tilde{A}_3(\mathbf{k}, \hat{G}^s(\epsilon))$ we substitute $\hat{G}^s(\epsilon)$ for ϵ^{-1} and multiply by ρ^2 yielding

$$\tilde{A}_3(\mathbf{k}, \hat{G}^s(\epsilon)) = \hat{G}^s(\epsilon)\rho^2 \int d\mathbf{r}_{12} \exp(i\mathbf{k}\cdot\mathbf{r}_{12}) \int d\mathbf{r}_{13} A(\mathbf{r}_{12}, \mathbf{r}_{13}, \hat{G}^s(\epsilon)), \tag{A13}$$

where

$$A(\mathbf{r}_{12}, \mathbf{r}_{13}, \hat{G}^s(\epsilon)) = \frac{\hat{G}^s(\epsilon)^{-1} w_{12} + w_{12}w_{13} + w_{12}w_{22} + w_{13}w_{23}}{\hat{G}^s(\epsilon)^{-2} + 2\hat{G}^s(\epsilon)^{-1}(w_{12}+w_{13}+w_{23}) + 3(w_{12}w_{13} + w_{12}w_{23} + w_{13}w_{23})} - \frac{w_{12}}{\hat{G}^s(\epsilon)^{-1} + 2w_{12}} . \tag{A14}$$

To calculate $\tilde{L}_3(\mathbf{k}, \hat{G}^s(\epsilon))$ we need the sum of all diagrams in the original $\hat{G}^m(\mathbf{k}, \epsilon)$ series [Eq. (42)] with three circles and a loop, which will be denoted $L_3(\mathbf{k}, \epsilon)$. $L_3(\mathbf{k}, \epsilon)$ can be generated from the diagrams in $\hat{G}^m(\mathbf{k}, \epsilon)$ which are linear in ρ, i.e., those diagrams with two circles. These diagrams are the same diagrams summed to give $\tilde{\sum}_2(\mathbf{k}, \hat{G}^s(\epsilon))$; the appropriate value of each diagram is given by Eq. (43). $L_3(\mathbf{k}, \epsilon)$ is generated from these diagrams by the substitution of a term in the density expansion of $\hat{G}^s(\epsilon)$ for ϵ^{-1}. The density expansion of $\hat{G}^s(\epsilon)$ in the thermodynamic limit is

$$\hat{G}^s(\epsilon) = \epsilon^{-1} + \rho B_2^s(\epsilon) + \rho^2 B_3^s(\epsilon) + \cdots . \tag{A15}$$

The term $\rho B_2^s(\epsilon)$ is the sum of all diagrams in $\hat{G}^s(\epsilon)$ with two circles, $\rho^2 B_3^s(\epsilon)$ the sum of all diagrams with three circles, etc. If we substitute the density expansion of $\hat{G}^s(\epsilon)$ for one ϵ^{-1} factor in a $\hat{G}^m(\mathbf{k}, \epsilon)$ diagram with two circles, the ϵ^{-1} term generates the original diagram with two circles, the first order term $\rho B_2^s(\epsilon)$ generates diagrams with three circles that contain a loop, the second order term generates diagrams with four circles and a loop, and the higher order terms generate diagrams with a loop and five or more circles. Thus the diagrams in $L_3(\mathbf{k}, \epsilon)$ can be generated by substitution of $\rho B_2^s(\epsilon)$ for one of the ϵ^{-1} factors in each of the $\hat{G}^m(\mathbf{k}, \epsilon)$ diagrams with two circles. For a diagram with n ϵ^{-1} factors there are n vertices where a loop can be inserted so we need to make this substitution for each ϵ^{-1} factor while leaving the other ϵ^{-1} factors unchanged; n equivalent terms describing the diagrams in $L_3(\mathbf{k}, \epsilon)$ which are generated from a single $\hat{G}^m(\mathbf{k}, \epsilon)$ diagram with two circles result. Equivalently we can replace each ϵ^{-1} factor by the density expansion of $\hat{G}^s(\epsilon)$ and keep only the n terms which are of the form $B_2^s(\epsilon)/\epsilon^{n-1}$. Using a summation procedure similar to that used to obtain $\tilde{\sum}_2(\mathbf{k}, \hat{G}^s(\epsilon))$ we get

$$L_3(\mathbf{k}, \epsilon) = \rho^2 B_2^s(\epsilon) \sum_{n=1}^{\infty} (-2)^{n-1} \left(\frac{n+1}{\epsilon^n}\right) \int d\mathbf{r}_{12} \exp(i\mathbf{k}\cdot\mathbf{r}_{12}) w_{12}^n$$

$$= \frac{2\rho^2 B_2^s(\epsilon)}{\epsilon} \int d\mathbf{r}_{12} \exp(i\mathbf{k}\cdot\mathbf{r}_{12}) \frac{w_{12}(1+\epsilon^{-1}w_{12})}{(1+2\epsilon^{-1}w_{12})^2} . \tag{A16}$$

$B_2^s(\epsilon)$ is found by exact solution of the finite volume two particle problem. The result is

$$B_2^s(\epsilon) = -4\pi^2 R_0^3 \epsilon^{-3/2} \tau^{-1/2}/(3 \cdot 2^{3/2}) \tag{A17}$$

and therefore

$$L_3(\mathbf{k}, \epsilon) = -\frac{2^{3/2}\pi^2 R_0^3 \rho^2}{3\epsilon^{5/2}\tau^{1/2}} \int d\mathbf{r}_{12} \times \exp(i\mathbf{k}\cdot\mathbf{r}_{12}) \frac{w_{12}(1+\epsilon^{-1}w_{12})}{(1+2\epsilon^{-1}w_{12})^2} . \tag{A18}$$

Substituting $\hat{G}^s(\epsilon)$ for ϵ^{-1} yields $\tilde{L}_3(\mathbf{k}, \hat{G}^s(\epsilon))$,

$$\tilde{L}_3(\mathbf{k}, \hat{G}^s(\epsilon)) = -\frac{2^{3/2}\pi^2 R_0^3 \rho^2 \hat{G}^s(\epsilon)^{5/2}}{3\tau^{1/2}} \times \int d\mathbf{r}_{12} \exp(i\mathbf{k}\cdot\mathbf{r}_{12}) \frac{w_{12}(1+\hat{G}^s(\epsilon)w_{12})}{(1+2\hat{G}^s(\epsilon)w_{12})^2} . \tag{A19}$$

The final step is to sum all diagrams in $\hat{G}^m(\mathbf{k}, \epsilon)$ [Eq. (42)] with three circles that contain a node, which will be denoted $N_3(\mathbf{k}, \epsilon)$. These diagrams can have only one node so they are a subset of the diagrams included in the quantity $\hat{G}_1^m(\mathbf{k}, \epsilon)$ defined by Eq. (58). As there are to be only three circles in the diagram there must be no loops in the diagram and the path to the node must contain no other circles. The second of these restrictions is satisfied by replacing $\tilde{\sum}(\mathbf{k}, \hat{G}^s(\epsilon))$ in Eq. (58) with $\tilde{\sum}_2(\mathbf{k}, \hat{G}^s(\epsilon))$. The first restriction is satisfied by replacing $\hat{G}^s(\epsilon)$ with ϵ^{-1} in $\tilde{\sum}_2(\mathbf{k}, \hat{G}^s(\epsilon))$ and Eq. (58). The result is

$$N_3(\mathbf{k}, \epsilon) = \frac{\rho^2}{\epsilon^3} \int d\mathbf{r}_{12} \exp(i\mathbf{k}\cdot\mathbf{r}_{12}) \times \int d\mathbf{r}_{13} \left(\frac{w_{13}}{1+2\epsilon^{-1}w_{13}}\right)\left(\frac{w_{32}}{1+2\epsilon^{-1}w_{32}}\right) \tag{A20}$$

and

$$\tilde{N}_3(\mathbf{k}, \hat{G}^s(\epsilon)) = \rho^2 \hat{G}^s(\epsilon)^3 \int d\mathbf{r}_{12} \exp(i\mathbf{k}\cdot\mathbf{r}_{12}) \times \int d\mathbf{r}_{13} \left(\frac{w_{13}}{1+2\hat{G}^s(\epsilon)w_{13}}\right)\left(\frac{w_{32}}{1+2\hat{G}^s(\epsilon)w_{32}}\right). \tag{A21}$$

We now have all the functions needed in the expression for $\tilde{\sum}_3(\mathbf{k}, \hat{G}^s(\epsilon))$, Eq. (A1).

To solve the self-consistency equation we need the $k=0$ value of the second approximation to $\tilde{\sum}(\mathbf{k}, \hat{G}^s(\epsilon))$, i.e., the sum of $\tilde{\sum}_2(0, \hat{G}^s(\epsilon))$, which is given by Eq. (84), and $\tilde{\sum}_3(0, \hat{G}^s(\epsilon))$. Evaluating Eq. (A1) at $k=0$ we get

$$\tilde{\sum}_3(0, \hat{G}^s(\epsilon)) = \rho^{-1}\hat{G}^s(\epsilon)^{-2}[\tilde{A}_3(0, \hat{G}^s(\epsilon)) - \tilde{L}_3(0, \hat{G}^s(\epsilon)) - N_3(0, \hat{G}^s(\epsilon))] . \tag{A22}$$

The three integrals to be evaluated are

$$\tilde{A}_3(0, \hat{G}^s(\epsilon)) = \hat{G}^s(\epsilon)\rho^2 \int d\mathbf{r}_{12} \int d\mathbf{r}_{13} A(\mathbf{r}_{12}, \mathbf{r}_{13}, \hat{G}^s(\epsilon)), \tag{A23}$$

$$\tilde{L}_3(0, \hat{G}^s(\epsilon)) = -\frac{2^{3/2}\pi^2 R_0^3 \rho^2 \hat{G}^s(\epsilon)^{5/2}}{3\tau^{1/2}} \times \int d\mathbf{r}_{12} \frac{w_{12}(1+\hat{G}^s(\epsilon)w_{12})}{(1+2\hat{G}^s(\epsilon)w_{12})^2} , \tag{A24}$$

and

$$\tilde{N}_3(0, \hat{G}^s(\epsilon)) = \hat{G}^s(\epsilon)^3 \rho^2 \int d\mathbf{r}_{12} \int d\mathbf{r}_{13} \times \left(\frac{w_{13}}{1+2\hat{G}^s(\epsilon)w_{12}}\right)\left(\frac{w_{32}}{1+2\hat{G}^s(\epsilon)w_{32}}\right) . \tag{A25}$$

The integral needed to obtain $\tilde{A}_3(0, \hat{G}^s(\epsilon))$ has been evaluated numerically by Haan.[10] Using his result we get

$$\tilde{A}_3(0, \hat{G}^s(\epsilon) = -0.80555\hat{G}^s(\epsilon)^2C^2\tau^{-1} . \quad \text{(A26)}$$

The integrations for $\tilde{L}_3(0, \hat{G}^s(\epsilon))$ can be done analytically. We find that

$$\tilde{L}_3(0, \hat{G}^s(\epsilon)) = -\frac{\pi\hat{G}^s(\epsilon)^2C^2}{2^{1/2}\tau}\int_0^\infty dx\,\frac{(1+x^{-6})}{x^4(1+2x^{-6})^2}$$

$$= -\frac{1.8506\hat{G}^s(\epsilon)^2C^2}{\tau} \quad \text{(A27)}$$

and

$$\tilde{N}_3(0, \hat{G}^s(\epsilon)) = \frac{\hat{G}^s(\epsilon)^2C^2}{2\tau}\left(\int_0^\infty \frac{dx}{1+x^2}\right)^2$$

$$= 1.2337\hat{G}^s(\epsilon)^2C^2\tau^{-1} . \quad \text{(A28)}$$

From these results and Eq. (A22) we obtain

$$\rho\tilde{\sum}_3(0, \hat{G}^s(\epsilon)) = -0.18870C^2\tau^{-1} . \quad \text{(A29)}$$

Including terms up to three-body in $\tilde{\sum}(\mathbf{k}, \hat{G}^s(\epsilon))$, the self-consistency equation is

$$\hat{G}^s(\epsilon) = \left[\epsilon + \frac{\pi C}{2\tau}\left(\frac{\tau}{2\hat{G}^s(\epsilon)}\right)^{1/2} - \frac{0.18870C^2}{\tau}\right]^{-1} . \quad \text{(A30)}$$

This can be written as a quadratic equation in $\hat{G}^s(\epsilon)^{1/2}$

$$\left[\epsilon - \frac{0.18870C^2}{\tau}\right]\hat{G}^s(\epsilon) + [\pi C/(2^{3/2}\tau^{1/2})]\hat{G}^s(\epsilon)^{1/2} - 1 = 0 . \quad \text{(A31)}$$

In addition to being a positive real number, $\hat{G}^s(\epsilon)^{1/2}$ must be a monotonically decreasing function of ϵ since a physically reasonable solution for the inverse transform, $G^s(t)$, must be a positive function of t. Only one of the two solutions to the quadratic equation has these properties. This solution is

$$\hat{G}^s(\epsilon) = \tau\left\{\frac{\pi^2C^2}{4}\left[1 - \left[1 + \frac{32}{\pi^2C^2}(\epsilon\tau - 0.18870C^2)\right]^{1/2}\right] + 4(\epsilon\tau - 0.18870C^2)\right\} \Big/ [4(\epsilon\tau - 0.18770C^2)^2] . \quad \text{(A32)}$$

For the second approximation to $\tilde{\sum}(\mathbf{k}, \hat{G}^s(\epsilon))$, $D(0, \epsilon)$ is given by

$$D(0, \epsilon) = (\pi CR_0^2\tau^{-1}/6)(2\hat{G}^s(\epsilon)/\tau)^{-1/6} + D_3(0, \epsilon) , \quad \text{(A33)}$$

where

$$D_3(0, \epsilon) = \lim_{k\to 0}\left\{(\rho/k^2)\left[\tilde{\sum}_\epsilon(0, \hat{G}^s(\epsilon)) - \tilde{\sum}_\epsilon(\mathbf{k}, \hat{G}^s(\epsilon))\right]\right\} . \quad \text{(A34)}$$

Using the method used to derive Eq. (93) we obtain

$$D_3(0, \epsilon) = A_3(\epsilon) - L_3(\epsilon) - N_3(\epsilon) , \quad \text{(A35)}$$

where

$$A_3(\epsilon) = \frac{\rho^2}{6\hat{G}^s(\epsilon)}\int d\mathbf{r}_{12}r_{12}^2\int d\mathbf{r}_{13}\,A(\mathbf{r}_{12}, \mathbf{r}_{13}, \hat{G}^s(\epsilon)) , \quad \text{(A36)}$$

$$L_3(\epsilon) = -\frac{2^{1/2}\pi^2R_0^3\rho^2\hat{G}^s(\epsilon)^{3/2}}{9\tau^{1/2}}\int d\mathbf{r}_{12}\,\frac{r_{12}^2w_{12}(1+\hat{G}^s(\epsilon)w_{12})}{(1+2\hat{G}^s(\epsilon)w_{12})^2} \quad \text{(A37)}$$

and

$$N_3(\epsilon) = \frac{\hat{G}^s(\epsilon)\rho^2}{6}\int d\mathbf{r}_{12}r_{12}^2\int d\mathbf{r}_{13} \times\left(\frac{w_{13}}{1+2\hat{G}^s(\epsilon)w_{12}}\right)\left(\frac{w_{32}}{1+2\hat{G}^s(\epsilon)w_{32}}\right) . \quad \text{(A38)}$$

The integral in $A_3(\epsilon)$ has been obtained numerically by Haan.[10] Using this result gives

$$A_3(\epsilon) = 0.064859C^2R_0^2\hat{G}^s(\epsilon)^{1/3}\tau^{-4/3} . \quad \text{(A39)}$$

The integrals for $L_3(\epsilon)$ and $N_3(\epsilon)$ can be done analytically,

$$L_3(\epsilon) = -\frac{3\pi C^2R_0^2\hat{G}^s(\epsilon)^{1/3}}{2^{3/2}\tau^{4/3}}\int_0^\infty dx\,\frac{(1+x^{-6})}{x^2(1+2x^{-6})^2}$$

$$= -0.94989C^2R_0^2\hat{G}^s(\epsilon)^{1/3}\tau^{-4/3} \quad \text{(A40)}$$

and

$$N_3(\epsilon) = \frac{C^2R_0^2\hat{G}^s(\epsilon)^{1/3}}{6\tau^{4/3}}\int_0^\infty dx\int_0^\infty dy\,\frac{x^{2/3}+y^{2/3}}{(x^2+2)(y^2+2)}$$

$$= 1.0362C^2R_0^2\hat{G}^s(\epsilon)^{1/3}\tau^{-4/3} . \quad \text{(A41)}$$

Therefore, from Eqs. (A33) and (A35)

$$D_3(0, \epsilon) = -0.02145C^2R_0^2\hat{G}^s(\epsilon)^{1/3}\tau^{-4/3} \quad \text{(A42)}$$

and

$$D(0, \epsilon) = (\pi CR_0^2\tau^{-1}/6)(2\hat{G}^s(\epsilon)/\tau)^{-1/6} - 0.02145C^2R_0^2\hat{G}^s(\epsilon)^{1/3}\tau^{-4/3} . \quad \text{(A43)}$$

[1](a) A. S. Davydov, *Theory of Molecular Excitons* (Plenum, New York, 1971); (b) D. M. Burland, V. Konzelmann, and R. M. Macfarlane, J. Chem. Phys. **67**, 1926 (1977); D. M. Burland, D. E. Cooper, M. D. Fayer, and C. R. Gochanour Chem. Phys. Lett. **52**, 279 (1977); (c) V. M. Kenkre and R. S. Knox, Phys. Rev. B **9**, 5279 (1974); Phys. Rev. Lett. **33**, 804 (1974); (d) M. Grover and R. Silbey, J. Chem. Phys. **52**, 2099 (1970); **54**, 4943 (1971).

[2](a) R. Kopelman, "Exciton Percolation in Molecular Alloys and Aggregates," in *Topics in Applied Physics*, Vol. 15, edited by F. K. Fong (Springer, New York, 1976); (b) J. R. Salcedo, A. E. Siegman, D. D. Dlott, and M. D. Fayer, Phys. Rev. Lett. **41**, 131 (1978); (c) R. D. Wieting, M. D. Fayer, and D. D. Dlott, J. Chem. Phys. **69**, 2752 (1978); D. A. Zwemer and C. B. Harris, *ibid.* **68**, 2184 (1978); (d) S. K. Lyo, T. Holstein, and R. Orbach, Phys. Rev. B **18**, 1637 (1978).

[3]J. Klafter and J. Jortner, Chem. Phys. Lett. **49**, 410 (1977).

[4]R. P. Hemenger and R. M. Pearlstein, J. Chem. Phys. **59**, 4064 (1973); F. W. Craver and R. S. Knox, Mol. Phys. **22**, 385 (1971) and references therein.

[5]R. M. Pearlstein, Proc. Natl. Acad. Sci. USA **52**, 824 (1964); T. Markvart, J. Theor. Biol. **72**, 91 (1978).

[6](a) Th. Förster, Ann. Phys. Leipzig **2**, 55 (1948); The quantity R_0 in Eq. (2) is the critical distance for the Förster rate. If two molecules, interacting only with each other, are separated by R_0 and one is excited, decay to the ground state and excitation transfer have equal probability; (b) D. L. Dexter, J. Chem. Phys. **21**, 836 (1953).

[7]S. Chandrasekhar, Rev. Mod. Phys. **15**, 1 (1943).

[8]S. W. Haan and R. Zwanzig, J. Chem. Phys. **68**, 1879 (1978).

[9]M. D. Frayer and C. R. Gochanour, J. Chem. Phys. (to be published).
[10]S. W. Haan, Ph.D. thesis, University of Maryland, College Park, Maryland, 1977.
[11]D. Förster, *Hydrodynamics, Fluctuations, Broken Symmetry, and Correlations Functions* (Benjamin, London, 1975).
[12]The generalized diffusion equation [Eq. (66)] is very similar in form to Dyson's equation in the quantum mechanical many-body problem. The function $\sum(\mathbf{k}, \hat{G}^S(\epsilon))$ is similar to the self-energy in Dyson's equation. See, for example, A. L. Fetter and J. D. Walecka, *Quantum Theory of Many Particle Systems* (McGraw-Hill, New York, 1971).
[13]H. Stehfest, Commun. Assoc. Comput. Mach. **13**, 47 (1970); **13**, 624 (1970).
[14]T. J. Chuang and K. B. Eisenthal, Chem. Phys. Lett. **11**, 368 (1971).
[15]H. C. Andersen, M. D. Fayer, and C. R. Gochanour, Phys. Rev. (to be published).